1 **Extreme warming rates affecting alpine areas in SW Europe deduced from algal**

2 **lipids**

4 Antonio García-Alix[1,2,3*], Jaime L. Toney[2], Gonzalo Jiménez-Moreno[1], Carmen Pérez-

5 Martínez[4], Laura Jiménez[4], Marta Rodrigo-Gámiz[1], R. Scott Anderson[5], Jon Camuera[6],

6 Francisco J. Jiménez-Espejo[3], Dhais Peña-Angulo[7], María J. Ramos-Román[6]

9 [1] Department of Stratigraphy and Paleontology, University of Granada, Granada, 18072,

10 Spain.

11 [2] School of Geographical and Earth Sciences, University of Glasgow, Glasgow, G12

12 8QQ, UK.

13 [3] Instituto Andaluz de Ciencias de la Tierra (IACT), CISC-UGR, Armilla, 18100, Spain.

14 [4] Department of Ecology and Institute of Water Research, University of Granada,

15 Granada, 18072, Spain.

16 [5] School of Earth and Sustainability, Northern Arizona University, Flagstaff, AZ 86011,

17 USA.

18 [6] Department of Geosciences and Geography, University of Helsinki, Helsinki, FI-00014,

19 Finland.

20 [7] Department of Geography, University of Zaragoza, Zaragoza, 50009 Spain.

22 * *Correspondence to:* Antonio García-Alix (agalix@ugr.es)

Abstract. Alpine ecosystems of the southern Iberian Peninsula are among the most vulnerable and the first to respond to modern climate change in southwestern Europe. While major environmental shifts have occurred over the last ~1500 years in these alpine ecosystems, only changes in the recent centuries have led to abrupt environmental responses, but factors imposing the strongest stress have been unclear until now. To understand these environmental responses, this study, for the first time, has calibrated an algal lipid-derived temperature proxy (based on long-chain alkyl diols) to instrumental historical data extending alpine temperature reconstructions to 1500 years before present. These novel results highlight the enhanced effect of greenhouse gases on alpine temperatures during the last ~200 years and the long-term modulating role of solar forcing. This study also shows that the warming rate during the 20th century (~0.18ºC/decade) doubled that of the last stages of the Little Ice Age (~0.09ºC/decade), even exceeding temperature trends of the high-altitude Alps during the 20th century. As a consequence, temperature exceeded the pre-industrial records in the 1950s, being one of the major forcings of the enhanced recent change in the alpine ecosystems from southern Iberia. Nevertheless, other factors reducing the snow and ice albedo (e.g., atmospheric deposition) may have influenced local glacier loss, since almost steady climate conditions predominated from middle 19th century to the first decades of the 20th century.

1. Introduction

Global mean annual surface temperatures have risen by ~0.85ºC from 1880 to 2012 and the recent decades have been the warmest in the Northern Hemisphere during the Common Era (IPCC, 2013). This trend is alarming, since over the last decade temperature records have been broken yearly. For example, in Spain the highest

49 temperatures ever recorded in September and July occurred in 2016 (45.5ºC) and 2017

50 (46.9ºC-47.3ºC), respectively (Spanish National Weather Agency - AEMet Open Data,

51 2019). Increasing global temperatures are contributing not only directly to land and ocean

52 surface warming, but are also changing the global hydrological cycle through the

53 disturbance of atmospheric circulation patterns and moisture (Easterling et al., 2000;

54 IPCC, 2013). As a result, the term "global warming" is migrating towards recent "climate

55 change" in order to express the variety of modern climate extremes witnessed across the

56 world. The effects of modern global warming and associated climate change events may

57 be causing extreme environmental impacts, beyond what is recorded in the recent

58 geologic record (Waters et al., 2016). Hence, it is crucial to identify warming thresholds,

59 rates, and forcing mechanisms from past high-resolution temperature records to

60 understand modern climate change. It is especially important in fragile regions such as

61 high elevation ecosystems of the Mediterranean alpine realm, an environmentally

62 vulnerable biodiversity "Hot-Spot" (Giorgi, 2006; Schröter et al., 2005) where recent

63 climate change is affecting species richness and distribution (Médail and Quézel, 1999;

64 Pauli et al., 2012). Therefore, alpine wetlands in the Mediterranean region, such as the

65 ones from the Sierra Nevada in the southern Iberian Peninsula, are sensitive recorders of

66 changing climate and their sedimentological records archive the ecological and

67 biogeochemical responses to different environmental forcings (Catalan et al., 2013).

68

69   In order to contribute to a better understanding of recent climate change events in

70 these vulnerable areas, here, for the first time, we calibrate a recently developed algal

71 lipid-derived temperature proxy in an alpine lacustrine record that overlaps with

72 instrumental temperature time-series. This calibration allows the reconstruction of

73 temperatures in alpine areas of the southern Iberian Peninsula during the Common Era

when instrumental records are discontinuous or non-existent. Temperature-dependent biomarkers, such as those produced by algae (alkenones) or bacteria/archaea (glycerol dialkyl glycerol tetraethers: GDGTs) have been commonly used in a wide range of marine records as quantitative paleothermometers, and their further application in lake environments has widely increased in the last decade (e.g., Castañeda and Schouten, 2011; Colcord et al., 2015; Foster et al., 2016; Longo et al., 2018; Theroux et al., 2010). Another promising type of algal lipid biomarkers, the long-chain alkyl diols (hereafter LCDs), have also been assessed as temperature proxy in marine areas (Rampen et al., 2014b; Rampen et al., 2012; Rodrigo-Gámiz et al., 2014; Rodrigo-Gámiz et al., 2015). Nevertheless, the relationship between LCDs and temperature has only been tentatively tested in freshwater environments (Rampen et al., 2014a). In this regard, studies using LCDs as (paleo)environmental proxies in marine environments (not just only for temperature reconstructions) have increased in the last years, showing the potential of LCDs as upwelling proxies (Rampen et al., 2008; Versteegh et al., 1997; Willmott et al., 2010), riverine inputs in marine settings (de Bar et al., 2016; Lattaud et al., 2017a; Lattaud et al., 2018a), or nutrient proxies (Gal et al., 2018). Nevertheless, only a few studies have tested them as lacustrine archives of paleoproductivity (Shimokawara et al., 2010), past rainfall anomalies (Romero-Viana et al., 2012), or temperatures (Rampen et al., 2014a), among others. In any case, despite the great potential of LCDs for paleoenvironmental reconstructions, a number of questions exist about the applicability of diols in high latitude areas (Rodrigo-Gámiz et al., 2015), in freshwaters records (Rampen et al., 2014a), and about the distribution and sources of the biological producers (Balzano et al., 2018; Villanueva et al., 2014; Yu et al., 2018), among others.

98   The LCD distribution in marine environments shows significant correlations with

99   mean annual sea surface temperature through the ratio of the fractional abundances of C_{28}

100   1,13-diol, C_{30} 1,13-diol, and C_{30} 1,15-diol that are used in the Long chain Diol Index (LDI,

101   Eq. (1)) (Rampen et al., 2012). The application of LCDs as a temperature proxy is novel

102   in freshwater environments and only two preliminary calibrations based on recent surface

103   sediments have been obtained using both mean annual air temperatures (weather station

104   data) and organic-derived temperature proxies (GDGTs) (Rampen et al., 2014a). Here,

105   we improve the biomarker paleothermometry by establishing the first temperature

106   calibration for freshwater LCDs using a comparison with historical temperature records

107   for the last ~100 years. Although this calibration can only be applied to the studied lake

108   at present, and perhaps to other alpine wetlands in the Sierra Nevada area, these new data

109   support and reinforce the promising use of LCDs as a paleotemperature proxy in

110   freshwater environments.

111

112   Equation (1) LDI= $(F_{C30}$ 1,15-diol)/$(F_{C28}$ 1,13-diol + F_{C30} 1,13-diol + F_{C30} 1,15-diol)

113   (Rampen et al., 2012)

114

115   **1.1 Regional settings**

116

117   This paper focuses on the LCD record of two adjacent cores from Laguna de Río

118   Seco (LdRS), a small alpine lake (~0.42 ha and less than 3m of water depth) at 3020 masl

119   in the protected Sierra Nevada National Park, southern Spain (Fig. 1). Alpine Sierra

120   Nevada wetlands, including LdRS, are low primary production (oligo-mesotrophic)

121   systems and their biogeochemical cycles partially depends on aeolian nutrient supplies

122 (e.g., Saharan aerosol deposition), since catchment basins are small and barren in

123 nutrients (Morales-Baquero et al., 2006; Pulido-Villena et al., 2005; Reche et al., 2009).

124

125   Sierra Nevada is the southwestern-most mountain range in Europe, where latest

126 Pleistocene cirque glaciers carved the metamorphic (mica schist) bedrock in the highest

127 peaks (Castillo Martín, 2009). Massive glacier melting at the latest Pleistocene-Holocene

128 transition transformed the former glacial depressions into lacustrine areas (Castillo

129 Martín, 2009) that evolved gradually into either shallow lakes or peatlands around the

130 middle-to-late Holocene transition (Garcia-Alix et al., 2017; Jiménez-Espejo et al., 2014).

131 Small glaciers re-appeared at the highest peaks of the Sierra Nevada in the 15th century,

132 during the Little Ice Age (LIA), and remained until the 20th century (Oliva et al., 2018).

133 The presence of these glaciers is observed in the sedimentary record in some alpine lakes

134 and wetlands in the Sierra Nevada as deposit of coarse sediments, like Laguna de la

135 Mosca on the north face of the Sierra Nevada (Oliva and Gomez-Ortiz, 2012). However,

136 these kinds of deposits have not been registered in LdRS (south face of the Sierra

137 Nevada), where the last 1500 years are characterised by continuous laminated clays and

138 bryophyte layers (Anderson et al., 2011). In any case, glacial effects have not caused any

139 disturbance on wetland sedimentation (e.g., erosion) and local alpine sedimentary records

140 show continuous sedimentation patterns (Anderson et al., 2011; García-Alix et al., 2012;

141 Jiménez-Moreno and Anderson, 2012; Jiménez-Moreno et al., 2013; Mesa-Fernández et

142 al., 2018; Oliva and Gomez-Ortiz, 2012; Ramos-Román et al., 2016). Conversely, an

143 increase in sedimentation rates have been detected in the last ~200 years, probably

144 resulting from the waning stages of the LIA (Oliva and Gomez-Ortiz, 2012) and enhanced

145 human activities in the alpines areas of Sierra Nevada during the 19th (García Montoro et

146 al., 2016; Titos Martínez, 2019; Titos Martínez and Ramos Lafuente, 2016) and 20th

147 (Jiménez et al., 2015) centuries. These high-sedimentation rates did not affect the natural

148 responses of the local algal communities to environmental variables such as temperature,

149 but with a primary effect of dilution of algal compounds (e.g., chlorophylls and labile

150 carotenoids) in the sediments (Jiménez et al., 2015).

151

152 During the 20th century this sensitive alpine region of southern Iberia has

153 experienced significant impacts from modern climate change as evidenced, for example,

154 by the first permanent European glacier loss there during the first half of the 20th century

155 (Grunewald and Scheithauer, 2010) and the extreme permafrost reduction during recent

156 decades (Oliva and Gomez-Ortiz, 2012). This melting supplied a large volume of

157 freshwater (Jiménez et al., 2019) that boosted the water availability in the area and the

158 occasional development of local aquatic environments, contrasting with the general

159 environmental aridification trend observed throughout the 20th century (Garcia-Alix et

160 al., 2017; Jiménez et al., 2019; Ramos-Román et al., 2016).

161

162 The sedimentary archive of LdRS has been selected for this study in order to 1)

163 improve the freshwater LCD paleothermometry by proposing a new temperature

164 calibration for freshwater LCDs in the alpine wetlands of the Sierra Nevada area, 2)

165 reconstruct temperatures beyond the instrumental record in a site at the leading edge of

166 changing climate, 3) assess the role of different radiative forcing (e.g., solar radiation or

167 greenhouse gas concentrations) on temperature change in alpine wetlands of the

168 southwestern Europe during the Common Era, and 4) understand the responses to recent

169 climate change in this highly sensitive environment.

170

171 **2. Materials and methods**

2.1. Sediment sampling

Two sediment cores were taken at the deepest part of LdRS, an alpine lake at 3020 masl in the Sierra Nevada (southern Iberian Peninsula) (Fig. 1). A long sediment core (150 cm) was retrieved in 2006 (LdRS lgc). A short sediment core of 16 cm was collected in 2008 (LdRS shc) using a slide-hammer gravity corer (Aquatic Research Instruments, Hope, Idaho, USA). Independent age models were performed in each sediment core to avoid potential correlation problems caused by changes in the sedimentation rates between both coring sites (Fig. 1c) and different sampling dates (2006-LdRS lgc and 2008-LdRS shc). The age model of LdRS lgc is based on ^{210}Pb and ^{137}Cs in the uppermost part (first 15 cm), and ^{14}C analyses in older sediments (Anderson et al., 2011). The age model of the LdRS shc is based on gamma spectroscopy by measuring the ^{210}Pb, ^{137}Cs, and ^{226}Ra radionuclides in the first ~14 cm, and afterwards the age was extrapolated to the core bottom (16 cm) (Jiménez et al., 2019; Jiménez et al., 2018). Both records show that the sediment accumulation rate for the uppermost 15-16 cm ranges between 0.09 and 0.13 cm/yr (Anderson et al., 2011; Jiménez et al., 2018), with lower sedimentation rates below this depth (~0.008 cm/yr) (Anderson et al., 2011). Ages models show that the LdRS shc extends back to ~200 years with a sample resolution ranging from 5 to 7 years (high-resolution) (Jiménez et al., 2019; Jiménez et al., 2018). In the case of the LdRS lgc, the section studied in this paper covers the last ~1500 years with a lower sample resolution. In this case, the sample resolution is around 6-7 years in the first 10 cm, and from 24 to 150 years in older samples (Anderson et al., 2011).

2.2. Geochemical analyses

197

Thirty-two sediment samples were collected consecutively every 0.5 cm along LdRS shc and twenty-one samples in the first 22 cm of LdRS lgc. The samples were freeze-dried and homogenized. The total lipid content was extracted from the sediment samples using a Thermo Scientific™ Dionex™ ASE™ 350 Accelerated Solvent Extractor system at 100ºC and 7×10^6 Pa using a mixture of dichloromethane (DCM) and methanol (9:1, v:v). Afterwards, the neutral fraction was separated by means of aminopropyl-silica gel chromatography using DCM:isopropanol (1:1, v:v). This neutral fraction was subsequently eluted with hexane, DCM, ethyl acetate:hexane (25:75, v:v), and methanol through a 230-400 mesh/35-70 micron silica-gel chromatographic column, in order to obtain four neutral sub-fractions (N1-N4). Long chain diols were obtained in the third neutral fraction (N3, alcohol fraction), which was derivatised by bis-(trimethylsilyl) trifluoroacetamide (BSTFA) before running the analyses. 30μL of BSTFA and 40μL of pyridine were added to each N3 fraction and heated at 80°C for 2 hours. When vials were at room temperature, a volume between 140 μl and 220 μl of DCM was added to each sample. Firstly, the derivatised N3 fractions were analysed with a Gas Chromatography with Flame-Ionization Detector (GC-FID Shimadzu 2010). An external standard of cholesterol was measured every five samples in order to estimate the proper concentration for mass spectrometry analyses. The sample at 19.5 cm depth in the long core was discarded because its concentration was below detection limits. Subsequently, the N3 fractions were measured in a Shimadzu QP2010-Plus Mass Spectrometer interfaced with a Shimadzu 2010 GC using a scan mode between m/z 50 − 650, in order to obtain a general picture of the mass spectrum of the samples and the specific retention times where the C_{28}, C_{30}, and C_{32} diols eluted. Afterwards, samples where re-analysed on the basis of a Selected-Ion Monitoring mode (SIM), selecting the

characteristic fragment ions of the most important long chain diols, i.e., *m/z* 299, 313, 327, and 341 (Rampen et al., 2012; Versteegh et al., 1997) and the specific retention time window to identify the C_{28}, C_{30}, and C_{32} diols with the mid-chain alcohol positioned at carbon 13, 14 or 15. Fractional abundances of the C_{28} 1,13-diol, C_{30} 1,13-diol, C_{30} 1,15-diol were used in Eq. (1) to calculate the Long chain Diol Index (LDI) (Rampen et al., 2012). Fractional abundances of C_{28} 1,13-diol, C_{30} 1,13-diol, C_{30} 1,15-diol and C_{32} 1,15-diol were used to characterise the potential diol source (e.g., marine, lacustrine, or specific algae groups) (Lattaud et al., 2018a; Rampen et al., 2014a). Fractional abundances of the C_{28} and C_{30} 1,14-diols were measured only in the short core in order to assess their potential relationship with temperatures (Rampen et al., 2014b). The presence of the $C_{32:1}$ 1,15-diol has also been tested, but it was only identified in some samples from the short core at very low concentrations, thus is not included it in this study.

2.3. Reference temperature time-series for LCD temperature calibrations

Generating an accurate temperature calibration based on LCDs in alpine wetlands from the Sierra Nevada area is challenging, because there is a lack of long and continuous temperature time-series at such high elevations. The meteorological observatories at the Sierra Nevada ski resort (ranging in elevation from 2500 to 3020 masl) only provided discontinuous temperature records from 1965 to 2011 (Observatorio del cambio global de Sierra Nevada, 2016; Spanish National Weather Agency - AEMet Open Data, 2019) that show a significant correlation (r>0.95; p<0.0001) with low elevation temperature time-series (Table S1, S2). Therefore, a potential way to obtain a LCD-based temperature calibration is by means of the correlation of LCD data with long and reliable historical

temperature time-series at nearby lower elevation areas, followed by a correction for the altitudinal effect on temperatures.

The three weather observatories in the Granada area, at the foothills of the Sierra Nevada, only provide reliable temperature data from the 1970s onwards (Spanish National Weather Agency - AEMet Open Data, 2019), which is a short-period for an accurate down-core proxy calibration. Temperature time-series from the 1970s backwards have been reconstructed using satistical models (e.g., Gonzalez-Hidalgo et al., 2015), showing a good correlation with the LDI and with the relative abundance of the C_{28} 1,13-, C_{30} 1,13-, and C_{32} 1,15-diols, with a weaker correlation for the C_{30} 1,15-diol (Table S3). However, these correlations are lower than the ones obtained from Sevilla-Tablada and Madrid-Retiro observatories. These observatories registered longer and more reliable temperature data than those obtained in Granada observatories, which are likely biased by the quality of the reconstructed temperature data. Therefore, after testing the correlations between LCDs and different low elevation observatories (Table S3), we decided to develop the LCD-based temperature calibrations against the temperature time-series from Sevilla-Tablada and Madrid-Retiro observatories. These observatories show the best correlations with the LCD data, in addition to being the most reliable and longest temperature time-series in the region (see Table S3 for further explanations and Fig. 1a for the location of these low-elevation observatories).

Another question to clarify in the study records before selecting the reference temperature time-series for the LCD calibration is the potential seasonal effect on the LCD distributions, since different studies have shown diverse relationships between annual or seasonal temperatures and the LCDs. For example, good correlations have been

found in marine environments between the fractional abundances of LCDs (expressed as LDI in all the cases) and annual (Rampen et al., 2012), winter and annual (Smith et al., 2013), or autumn and annual sea surface temperatures (Lattaud et al., 2018b). Despite fewer studies on the LCD distribution in freshwater environments, Rampen et al. (2014a) found a good correlation between the LCD distributions in a suite of lake surface sediments and mean summer lake temperatures (deduced from GDGTs). Nevertheless, the direct correlation between these LCD distributions and annual or seasonal air temperatures was weaker, probably due to the location of the weather observatories with respect to each study area. Villanueva et al. (2014) also investigated this seasonal effect and detected changes in the LCD distribution throughout the year in the water column and surface sediments from an African lake that could be either related to successive and different LCD-producer blooms or seasonal variations in the LCD production by a unique source. Both scenarios might affect LCD-based temperature reconstructions.

Considering all these constrains to select the best temperature time-series to establish an accurate LCD-based temperature calibration, the most rigorous approach for the studied alpine site would consider annual and monthly water and/or air temperatures of the catchment basin at 3020 masl, as well as, the periods of the year when the LCDs are produced, but these data are not available so far. Thus, the effect of seasonality has been estimated by means of the comparison with reliable seasonal long temperature time-series from lower elevation sites. In this regard, seasonal air temperatures for the last ~100 years registered in Madrid and Sevilla observatories correlate with the LCD distributions (with a weaker correlation for the C_{30} 1,15-diols) and the LDI ($0.9>r>0.6$; $p<0.001$). Nevertheless, this correlation is generally lower than the one obtained when considering only mean annual air temperatures (MAAT) (i.e., in the case of the LDI vs MAAT $r=0.9$;

296   *p*<0.0001). Since warm temperatures influence the algae growth in the studied area

297   (Carrillo et al., 1991; Sánchez-Castillo, 1988), we would expect a higher correlation

298   between LCDs and mean seasonal air temperatures from the warmer months (MWAT:

299   May-September), which is potentially the LCD production season, but this correlation is

300   lower than the annual ones in the case of the LDI (LDI *vs* MWAT $0.8>r>0.7$; *p*<0.0001)

301   (Table S3, S4). A similar pattern is observed when annual and warm season temperatures

302   are compared with the fractional abundances of the C_{28} 1,13-, C_{30} 1,13-, C_{30} 1,15-, and

303   C_{32} 1,15-diols (Table S3). Consequently, in view of 1) the fact that this is the first attempt

304   at a freshwater LCD-based temperature calibration in this area; 2) there exists a high

305   correlation between the different instrumental time-series of regional air temperatures

306   (seasonal *vs* annual), and 3) the best correlations (normal and detrended) between the

307   LCD distributions and temperatures are obtained when using MAAT (Tables S3, S4), we

308   use MAAT for the LCD-based temperature calibrations in this study. Nevertheless,

309   further work, including a monitoring program for monthly air temperatures in the

310   catchment area and water temperatures at the lake, as well as, suspended particulate

311   matter and sediment trap studies, is needed to better understand the seasonal LCD

312   production and the biological sources, providing more constrains to improve the current

313   LCD-based temperature calibration.

314

315   Two groups of reference temperature time-series at 3020 masl, based on the same

316   batch of data, have been estimated in order to overcome the scarcity of high-elevation

317   temperature time-series in the Sierra Nevada and obtain a reliable mean LCD-based

318   temperature calibration: 1) based on the elevational gradient between low and high

319   elevation observatories and 2) based on the direct correlation between temperature time-

320   series from Madrid and Sevilla observatories and that at 3020 masl (Cetursa 5

321 observatory) in the Sierra Nevada, which is near LdRS and at the same elevation (Table

322 S1).

323

324   Reference temperature time-series 1: The environmental lapse rate

325 ($\Delta_{temperature}/\Delta_{elevation}$ in ºC/m) between lower elevation observatories (with long

326 temperature time-series: Granada, Sevilla, and Madrid) and those from Sierra Nevada at

327 higher elevation (with shorter temperature time-series: Albergue, and Cetursa 1, 3 and 5)

328 has been estimated in order to correct the elevational gradient between them (more than

329 2200 m: Table S1). Due to few annual data points from high elevation sites, monthly and

330 annual (twelve continuous months) environmental lapse rates were calculated to compare

331 both datasets. The calculated temperature shifts between the reference low elevation

332 observatories and LdRS site at 3020 masl, worked out from Fig. S1 equations (Table S5),

333 was applied to the temperature time-series from Madrid and Sevilla for the last ~100 years

334 in order to obtain two reference temperature reconstructions (from 1908 to 2008 CE) at

335 3020 masl: reference temperature time-series 1a (from Madrid data), and reference

336 temperature time-series 1b (from Sevilla data).

337

338   Reference temperature time-series 2: The direct comparison between Madrid and

339 Sevilla temperatures and those from the observatory Cetursa 5 (3020 masl) by means of

340 ordinary least square regressions has given rise to two equations (Fig. S2a and b) that

341 allow the reconstruction of temperature time-series at 3020 masl from 1908 to 2008:

342 reference temperature time-series 2a (from Madrid data), and reference temperature time-

343 series 2b (from Sevilla data).

344

345   As a result, we have obtained four reference temperature time-series at 3020 masl

346   where the effect of the altitudinal difference between low elevation observatories (Madrid

347   and Sevilla) and LdRS have been corrected by two different methods. Consequently,

348   these four reference temperature series are highly similar, showing a certainly high

349   correlation ($r>0.98$; $p<0.0001$), without significant difference between the sample

350   medians (deduced from a Kruskal-Wallis test), and very low standard deviation between

351   samples from the same time interval (SD 0.2).

352

353   **3. Results**

354

355   **3.1. Long chain diols in the LdRS records**

356

357   Six main LCD isomers have been identified and relatively abundances analysed

358   in the LdRS cores: C_{28} and C_{30} 1,13-diols, C_{28} and C_{30} 1,14-diols, and C_{30} and C_{32} 1,15-

359   diols. Their relative abundance changes through time in both records, but the C_{32} 1,15-

360   diol is the predominant isomer in most of the samples. Nevertheless, the relative

361   abundance of the C_{32} 1,15-diol drops abruptly (relative abundances between 25% and

362   40%) during the LIA, contrasting with a relative increase in the C_{28} and C_{30} 1,13-diols

363   (Fig. 2). This switch in the most abundant isomers can be read as either a change in the

364   LCD producers or an adaptation to colder temperatures of the same organism, and thus

365   affecting the LCD production. Conversely, the C_{28} and C_{30} 1,14-diols show the lowest

366   relative abundances ($1.3 \pm 0.4\%$ and $1.8 \pm 0.3\%$, respectively). They were only quantified

367   in the short core to assess their potential application as paleothermometer in LdRS.

368   Although they show a good correlation with temperatures (C_{28} 1,14-diol: $0.66>r>0.45$

369     $p<0.04$; C_{30} 1,14-diol: $-0.82<r<-0.53$ $p<0.02$), their low relative abundance, very close to

370 the detection limit, together with a different biological source (Sinninghe Damsté et al.,

371 2003), preclude us from including them in the temperature calibration, and therefore, in

372 the discussion of this study. Consequently, the interpretations in this paper are only

373 focused on the distribution pattern of the relative abundances of the main LCDs in LdRS:

374 C_{28}-C_{30} 1,13-diols and C_{30}-C_{32} 1,15-diols.

375

376   The relative abundances of these four isomers in LdRS correlate well in both short

377 and long cores, only C_{30} 1,15-diol showing weaker correlations with the other isomers

378 (Table S6). Overall, C_{28} and C_{30} 1,13-diols show opposite trends to those from the C_{30}

379 and C_{32} 1,15-diols. Their general trends for the last ~100 years seem to be influenced by

380 the temperature oscillations at 3020 masl (Table S7): the C_{28} and C_{30} 1,13-diols display a

381 negative correlation with temperatures (r<-0.7 p<0.0001) and the C_{32} 1,15-diol a positive

382 one (r>0.8 p>0.0001). Although the C_{30} 1,15-diol also shows a positive relationship with

383 temperatures, this correlation is weak (r>0.3 p>0.0001). Accordingly, the LDI values

384 from LdRS for the last ~100 years show a significant correlation (r>0.9 p>0.0001) with

385 the reference temperature time-series at 3020 masl (Table S7).

386

387   The different diol isomers in LdRS also show good agreement with general

388 temperature trends during the last ~1500 years. The C_{30} and C_{32} 1,15-diols depict a

389 positive relationship with temperatures, whereas the C_{28} and C_{30} 1,13-diols display a

390 negative one. Thus, the LDI record obtained from the C_{28}-C_{30} 1,13-diols, and C_{30} 1,15-

391 diol also show important fluctuations during the last ~1500 years, in agreement with the

392 general temperature trends of the Common Era (CE). More specifically, LDI values in

393 the LdRS lgc range from ~0.23 to 0.05 from ~400 to 1900 CE, with maximum and

394 minimum values recorded at ~930 and ~1690 CE, respectively (Fig. 3). These changes

395   are coeval with the minimum temperatures of the LIA and the maximum temperatures of

396   the Medieval Climate Anomaly (MCA). LDI fluctuations were extremely abrupt during

397   the 20th century, ranging from 0.10 to 0.31 in the lowest resolution LdRS lgc record and

398   from 0.13 to 0.32 in the highest resolution LdRS shc record. These minimum and

399   maximum values were reached in both cases during the first and last decades of the 20th

400   century, respectively (Fig. 3).

401

402   **3.2. LCD temperature calibration**

403

404   A total of twenty-six samples from both short and long LdRS cores ranging in age

405   from 1908 to 2008 were selected to perform the LCD-based temperature calibration,

406   along with the two groups of reference temperature time-series at 3020 masl. Since

407   sedimentary samples used in the calibration have a time averaging between 5 and 7 years,

408   a mean of the historical temperatures covering the same time averaging of each sample

409   was calculated.

410

411   Eight different calibrations have been performed: five using the LDI, one using a

412   multiple linear regression of the relative abundances of C_{28} 1,13-diol, C_{30} 1,13-diol, and

413   C_{30} 1,15-diol (following Rampen et al., 2014a) (MLR calibration 1 hereafter), one using

414   multiple linear regressions of the ratios of the relative abundances of LCDs with positive

415   (even weak) correlation with temperature against the ones with negative correaltion (C_{30}

416   1,15- / C_{28} 1,13-diols; C_{30} 1,15- / C_{30} 1,13-diols; C_{32} 1,15- / C_{28} 1,13-diols; and C_{32} 1,15-

417   / C_{30} 1,13-diols) (MLR calibration 2 hereafter), and one using multiple linear regressions

418   of the ratios of the relative abundances of C_{30} 1,15- / C_{28} 1,13-diols and C_{30} 1,15- / C_{30}

419   1,13-diols (MLR calibration 3 hereafter). The statistics and the equations for the MLR

420   calibrations 1, 2, and 3 are described in the Table S8.

421

422   In the case of the LDI, ordinary least square regressions were run between the four

423   reference temperature time-series at 3020 masl and the LDI record from LdRS shc and

424   lgc, resulting in four calibration equations (Fig. S3). The slopes of these four equations

425   range from 8.2 to 10.2. The LDI-derived temperatures from the reference time-series 2

426   show the highest values for the last ~100 years, whereas the minimum values are mainly

427   shown by the ones calculated with the reference time-series 1. The difference between

428   the four LDI-derived temperatures for the last ~100 years is low, with a standard deviation

429   lower than 0.13. The standard error of these four individual calibrations ranges from 0.18

430   to 0.23ºC, and the maximum residual is ~0.8ºC. However, due to the uncertainty of

431   establishing an accurate temperature time-series at 3020 masl, LDI-derived temperature

432   values from these LDI individual calibrations have been used to determine the range of

433   the variation (minimum and maximum temperature values) for each point, and an

434   additional calibration, summarising the relationship between LDI and the four reference

435   temperatures at 3020 masl has been performed. The obtained 104 combinations of LDI

436   and temperature data provided an equation representing the average relationship between

437   MAAT and LDI (Eq. (2); Fig. 4a). Since this is a summary of the four temperature time-

438   series, the residual errors include the residual errors of the individual LDI calibrations

439   (Fig. S3). The residual errors of this average temperature calibration, according to both

440   the LDI-reconstructed temperatures and the reference temperature time-series, are lower

441   than 0.8ºC (similar to the four individual LDI calibrations), with the standard error of

442   0.28ºC. The histogram showing the frequency of the residuals reveals that the ~85% of

443   the residuals range from 0.4 to -0.4ºC. This percentage is slightly lower (~62%) when the

444   residual interval is established between 0.2 and -0.2ºC (Fig. 4b). Only one data point from

445   1973 among the 104 data combination may be an outlier since it shows a residual 2.5

446   times higher than the residual standard deviation.

447

448   Equation (2) MAAT (ºC) = 9.147 x LDI - 0.243   (n = 26 x 4; r^2 = 0.79)*

449   * n = 26 LDI values plotted against four reference temperature time-series providing a

450   total of 104 combinations.

451

452   All the calibrations (LDI and MLR calibration 1, 2, and 3) show good correlation

453   with temperatures (Fig. 4 for LDI and Table S8 for MRL calibrations 1, 2, and 3). The

454   obtained temperatures from the average LDI calibration and those using multiple linear

455   regressions depict very similar trends in both cores (Fig. S4; r>0.96; p<0.0001).

456   Nevertheless, the correlation is slightly lower (r>0.82; p<0.0001) for the results from

457   MLR calibration 1 in the long core. In addition, some inconsistencies come up in the

458   reconstructed temperatures from MLR calibration 1: in general, temperatures tend to be

459   lower than those from the other calibrations, giving rise to negative annual values during

460   the LIA. This would be highly unlikely since under this scenario the lake would have

461   stayed frozen all year round, with little or no sedimentation occurring. Temperature

462   reconstructions using MLR calibrations 2 and 3 take the advantage of the ratios of isomers

463   with positive *vs* negative relationship with temperatures. The results are similar to the

464   ones obtained with the LDI, except for the LIA. Nevertheless, we discarded MRL

465   calibration 2 as it also uses the C_{32} 1,15-diol, whose relationship with temperature is not

466   clear, only reporting a positive correlation in some culture studies (Rampen et al., 2014b).

467   MRL calibration 3 provides the most similar results to those from the LDI, especially

468   comparing the temperature anomalies of both records with respect to the last 30 years of

the record, showing differences of less than ~0.1ºC. However, this difference increases (~0.3ºC) in the LIA. As this is the first study of LDI in sedimentary records from alpine lakes of the Sierra Nevada area, we have opted for a conservative solution following the LDI temperature calibration. The temperature reconstructions from MRL calibration 1, 2, and 3 will only be mentioned when needed in the discussion.

The application of the obtained calibration to the LDI values of LdRS (Eq. 2) produced the first temperature reconstruction for the Common Era in this alpine area (Fig. 3). In order to estimate the real magnitude of temperature variations during this period, the mean annual air temperature anomaly (MAATA ºC) has been calculated with reference to the annual MAAT of the last 30 years of the record (2008-1979). The lowest temperatures were recorded between ~1600 and ~1780 CE, with a temperature anomaly ranging from ~ -1.9 to ~ -2.2ºC. These temperature anomalies only reached positive values after 1998 (Fig. 3).

4. Discussion

4.1. Long chain diol distribution in alpine lakes from southern Iberia

The distribution pattern of the main LCDs in LdRS (C_{28}, C_{30} 1,13- and C_{30}, C_{32} 1,15-diols) could help us decipher the potential biological producers. There is a high percentage of the C_{32} 1,15-diol, which is one of the main features observed in freshwater environments (Lattaud et al., 2018a; Rampen et al., 2014a) (Fig. 2, S5). Another relevant feature of the distribution of the LCDs in LdRS is the low and constant relative abundance of the C_{30} 1,15-diol (6.5 $\pm$ 1.5%) throughout the LdRS records (Fig. 2), agreeing with the

range of the most probable distribution of C_{30} 1,15-diol in marine algae (Fig. S5; Table S9). This feature is not common in marine or lake sediments (de Bar et al., 2016; Lattaud et al., 2017a; Rampen et al., 2014a), resulting in an almost unique area for LdRS isomers (most specifically C_{28} 1,13-, C_{30} 1,15-, and C_{32} 1,15-diols) when comparing with literature data in a ternary diagram (Fig. 2). Conversely, the distribution of both C_{28} and C_{30} 1,13-diols usually shows similar patterns as other freshwater samples (Lattaud et al., 2018a; Rampen et al., 2014a) (Fig. 2, S5, Table S9). A Kruskal-Wallis ANOVA test was used to assess whether the distribution of the main LCDs in LdRS and from other sources (e.g., marine, freshwater, algal culture) were statistically different. Results point towards no significant differences between the whole LCD distribution in LdRS and the other sources. Nevertheless, the Kruskal-Wallis test found significant differences among individual isomers of the different sources (including LdRS). Subsequently, a Mann-Whitney U test was performed to compare pair of groups (individual isomers from LdRS *vs* individual isomers from source 1, 2, and so on), finding significant differences among most of them (Table S9). All these evidences suggest that the LCD distribution in the LdRS might differ from those of previous studies published to date and the potential biological producers at LdRS would be thus uncertain.

Eustigmatophyceae algae (e.i. *Vischeria* sp., *Eustigmatos* sp.) have been commonly proposed as the main diol producers in freshwater environments dominated by a mix of C_{28} 1,13-, C_{30} 1,15-, and C_{32} 1,15-diols (Rampen et al., 2014a; Villanueva et al., 2014; Volkman et al., 1999). Moreover, a dominance of C_{32} 1,15-diol has been identified in families of Goniochloridaceae and Monodopsidaceae (Lattaud et al., 2018a; Rampen et al., 2014a). Nevertheless, planktonic algae communities are very simple in the alpine Sierra Nevada wetlands (Sánchez-Castillo, 1988) and Eustigmatophyceae algae

have not been identified so far (Barea-Arco et al., 2001; Sánchez-Castillo, 1988). Thus, this study suggests that LCD producers in LdRS might be different from those identified previously in other freshwater environments and algal culture studies, making the potential source of LCDs even more complex than originally thought. Consequently, the outcomes of this paper (i.e., the LCD-based temperature calibration) should not be generally applied to other freshwater records unless they show a similar LCD distribution as LdRS. Additional research combining lipids and 18S rRNA gene sequencing analyses from suspended particulate matter, surface sediments, and sediment traps would be needed to unravel the real biological sources of LCDs in these alpine wetlands.

4.2. LdRS record in the environmental context of the Iberian Peninsula during the Common Era

Abrupt changes in temperature and precipitation have been depicted during the last 2000 years in the Iberian Peninsula and surrounding marine areas (Moreno et al., 2012; Sánchez-López et al., 2016). Precipitation was highly variable, showing arid conditions during the MCA, especially in southern Iberia, overall humid conditions throughout the LIA (with a complex internal structure showing large variability in humidity and extreme events), and arid conditions for the Industrial Period (Moreno et al., 2012; Oliva et al., 2018; Rodrigo et al., 1999; Sánchez-López et al., 2016), especially in high elevation wetlands from southern Iberia (Anderson et al., 2011; Garcia-Alix et al., 2017; Jiménez-Espejo et al., 2014).

Although the Early Middle Ages displayed a great temperature variability in the Iberian Peninsula and surrounding marine sites (Moreno et al., 2012; Sánchez-López et

544 al., 2016), three main stages have been identified for the last millennium deduced from
545 different proxies: a warm period throughout the MCA followed by cold temperatures
546 during the LIA, ending in an abrupt warming in the second half of the 20th century
547 (Moreno et al., 2012; Oliva et al., 2018; Sánchez-López et al., 2016). One of the proxies
548 used to reconstruct such temperature variations in continental areas of the Iberian
549 Peninsula has been tree ring data. Long tree ring temperature archives of the Iberian
550 Peninsula showed the same overall variations as the ones registered in LdRS, such as high
551 temperatures before 1250 CE (Büntgen et al., 2017), some temperature declines coeval
552 with solar minima during the LIA (e.g., the end of Spörer or Maunder Minima), as well
553 as a period of moderate-low temperatures from ~1850 to ~1940, followed by an
554 increasing temperature trend in the second half of the 20th century with several
555 temperature drops between ~1960 and ~1990 (Büntgen et al., 2017; Tejedor et al., 2017).
556 Nevertheless, the warming documented from the LCD-derived temperatures in the last
557 stages of the LIA is more pronounced in the LdRS record. The same overall trends have
558 been observed in European summer temperatures deduced from tree ring records
559 (Luterbacher et al., 2016) (Fig. 5b, d, and 6b, c). Surprisingly, tree ring data from the
560 Pyrenees and other Iberian areas show minor temperature variations, and even a slight
561 temperature decrease from ~2000 to 2008 similar to the one observed in the LCD-derived
562 temperatures from the LdRS record (Fig. 4c). This temperature stabilization at the
563 beginning of the 21st century is coeval with globally reduced warming rates over the
564 2001–2014 period (Fyfe et al., 2016).

565

566 Contrasting with these continental temperature reconstructions, high-resolution
567 sea surface temperature (SST) estimations from marine sites surrounding the Iberian
568 Peninsula, such as those derived from alkenones ($U^{K'}_{37}$) in the Tagus Delta (Iberian

569 Atlantic Margin) or in the Balearic Islands (western Mediterranean Sea), showed a

570 general decreasing trend for the last ~2000 years, with a warm MCA, a cold LIA, and

571 cold/moderate temperatures for the Industrial Period that do not appear to mirror the

572 modern global warming observed throughout the 20th century (Abrantes et al., 2005;

573 Moreno et al., 2012). Only high-resolution $U^{K'}_{37}$-and TEX_{86}-derived (from GDGTs) SST

574 records of the cores 384B and 436B from the Alboran Sea (Nieto-Moreno et al., 2013)

575 and the $U^{K'}_{37}$-SST record of core Gol-Ho1B from the Gulf of Lion (Sicre et al., 2016)

576 have shown a clear temperature increase during the 20th century, similar to the LDI

577 temperature record in LdRS (Fig. 5a,d, 6a,c). The observed heterogeneity in the SST

578 reconstructions based on different biomarkers such as alkenones (Abrantes et al., 2005;

579 Moreno et al., 2012; Rodrigo-Gámiz et al., 2014), GDGTs (Nieto-Moreno et al., 2013) or

580 LCDs (Rodrigo-Gámiz et al., 2014) could be explained since each record belongs to a

581 different biogeographical area influenced by specific temporal and dynamic

582 oceanographic regimes, as well as by different primary productivity patterns of each

583 biological source (e.g., seasonality or bloom length) (Sicre et al., 2016).

584

585   The previously described climate variability in precipitation and temperature

586 during the last ~1500 years in the Iberian Peninsula have been explained by different

587 forcing mechanisms such as the effect of the westerlies-North Atlantic climate dynamics,

588 internal climate variability, solar irradiance, volcanism, or anthropogenic forcing

589 (Gómez-Navarro et al., 2011; Gómez-Navarro et al., 2012; Moreno et al., 2012; Sánchez-

590 López et al., 2016). Their potential effect on the LCD distribution in the LdRS records is

591 discussed in the following section.

592

4.3. Control mechanisms on alpine temperatures in SW Europe during the

Common Era

This discussion is based on the LDI-temperature reconstruction. However, similar results are obtained when comparing the temperature reconstructions from MLR calibrations 1, 2, and 3 in LdRS and the different forcing mechanisms assessed in this section (Tables S10-S13).

Solar, volcanic, and anthropogenic (e.g., CO_2 and CH_4) radiative changes, along with the internal variability are usually attributed as the leading factors controlling temperatures during the Common Era (Ammann et al., 2007; IPCC, 2013). In addition, North Atlantic climate dynamics such as the North Atlantic Oscillation (NAO) or the Atlantic Multidecadal Oscillation (AMO) are other potential drivers of natural climate variability in the Iberian Peninsula (López-Moreno et al., 2011; Moreno et al., 2012; O'Reilly et al., 2017; Sánchez-López et al., 2016). The control of the North Atlantic climate dynamics in the studied alpine wetlands is evident, at least for precipitation and humidity fluctuations, since the NAO and solar forcing have been described as the main controls on the paleoenvironmental evolution recorded in this area (Garcia-Alix et al., 2017; Ramos-Román et al., 2016). Conversely, other studies have shown that the NAO climate mode had little effect on temperatures in this alpine area from 1950 to 2006 CE (López-Moreno et al., 2011). LdRS data agree with this observation, since no correlation (Tables S10-S13) has been detected between the NAO reconstruction (Trouet et al., 2009) and the obtained LCD record for the last millennium. The AMO has an impact on the North Atlantic atmospheric blocking mechanisms (Häkkinen et al., 2011) and on the European and Mediterranean temperatures, especially during the AMO warm phases

618   (O'Reilly et al., 2017). In the study area, the AMO shows a moderate long-term

619   correlation (Figs. 5d,e and 6c,d $r>0.60$; $p<0.01$) with both long and short core derived-

620   LDI records, but the correlation decreases when long-term trends are removed ($r<0.32$;

621    $p>0.1$) (Tables S10, S11). Since the nature of the AMO and its specific drivers are still

622   a matter of debate, i.e., internal ocean variability control (multidecadal fluctuations in

623   the Atlantic Meridional Overturning Circulation) versus solar or volcanic forcing for

624   the last centuries (Knudsen et al., 2014), we cannot conclude whether the observed

625   correlations represent the sole effect of the AMO or the influence of its underlying

626   forcing mechanisms.

627

628   The significant correlation at long and short terms ($r>0.61$; $p<0.005$) between

629   LDI-derived temperatures from LdRS records and greenhouse gases (Schmidt et al.,

630   2011) (Fig. 6c, g; Table S10), especially since the beginning of the 20th century (Industrial

631   Period) (Fig. 5d,g; Table S11), suggests that greenhouse gases might have an important

632   effect on temperatures at this high elevation site.

633

634   The potential impact of solar radiation and volcanic eruptions on climate over both

635   short- and long-time scales is a topic of controversy in the literature (Ammann et al.,

636   2007). In this regard, volcanic forcing, which should give rise to negative radiative

637   forcing in the climate system (Ammann et al., 2007; Sigl et al., 2015), do not show a

638   significant correlation with LDI-derived temperatures from LdRS records over the last

639   1500 years (Figs. 5d,h and 6c,h; Table S10, S11). We suggest that this lack of influence

640   at LdRS records is a function of its high-altitude location, at 3020 masl, in the free

641   troposphere, which reduces the environmental impact of small volcanic tropospheric

642   eruptions that likely have greater effects on lower elevation sites (Mather et al., 2013). In

643   addition, the relatively short residence time of volcanic aerosols in the atmosphere mainly

644   causes, at most, decadal-timescale effects (Sigl et al., 2015) that can be difficult to identify

645   in most sedimentary records due to the age resolution, as in the case of older sediments

646   than 200 years in LdRS. Nevertheless, large explosive volcanic eruptions delivering large

647   amounts of stratospheric aerosols (Marotzke and Forster, 2015; Sigl et al., 2015), such as

648   that for Agung Volcano in Bali, Indonesia (1963-1964 CE), may be associated with a

649   small depression in LDI-derived temperatures observed in LdRS records (Fig. 5d,h).

650   Although cold LDI-reconstructed temperatures occasionally seem to occur coevally with

651   volcanic eruptions, for example, 560-510 and 320 years ago (~1450-1500 and 1690 CE)

652   (Sigl et al., 2015), there is no consistent relationship between the intensity - number of

653   large eruptions and the reconstructed coolings in LdRS records, especially over the last

654   ~200 years when the age sample resolution would be enough to detect them (LdRS shc).

655

656   Most of the above-mentioned cooling events recorded in LdRS, such as those

657   during the LIA, are coeval with low solar activity periods like the Spörer Minimum (from

658   ~1450 to 1550 CE) or the Maunder Minimum (from ~1645 to 1715 CE) (Stuiver and

659   Quay, 1980) (Fig. 6). Thus, long-term correlations between LDI-derived temperatures

660   and solar activity, based on reconstructions of the solar irradiance and cosmogenic

661   isotopes (such as ^{14}C), are evident during the last ~1500 years in LdRS record (r>0.69; p

662   <0.002) (Fig. 6c,e,f; Table S11). This correlation drops (0.37< r <0.56 and 0.04< p <0.14)

663   when long-term trends are removed (Table S11). The long-term solar influence agrees

664   with previous observations in other alpine records of this area (Garcia-Alix et al., 2017;

665   Ramos-Román et al., 2016). Solar activity slightly decreases its long-term influence in

666   LdRS record during the last ~200 years (r>0.56; p<0.001) and disappears when long-term

667   trends are removed (Table S10). Only some occasional temperature decreases or slower

668   rates of warming such as during the 19th to 20th century transition, from ~1930 to 1940,

669   from ~1960 to 1975, and around 1988 CE, are coeval with slight declines in the total solar

670   activity (Fig. 5d,f: blue arrows).

671

672   In the same way, LdRS registered a small decrease in LDI-derived temperatures

673   (or stabilization) at the beginning of the 21st century (Fig. 5d), also recorded in the Madrid

674   and Sevilla temperature time-series (Spanish National Weather Agency - AEMet Open

675   Data, 2019), and thus in the reconstructed reference temperatures time-series at 3020 masl

676   (Fig. 5c), in tree ring records of the the Pyrenees and Iberian Range (Büntgen et al., 2017;

677   Tejedor et al., 2017), in marine platforms of the western Mediterranean (Fig. 5a) (Sicre

678   et al., 2016), and globally (Fyfe et al., 2016). Although this slowdown agrees with a

679   decreasing trend in solar activity and a slight stabilization of atmospheric methane

680   concentrations (Fig. 5f,g), the causes are more complex, and probably related to a

681   combination of internal variability and radiative forcing (e.g., volcanic and solar

682   activity, or decadal timescale changes in anthropogenic aerosols) (Fyfe et al., 2016).

683

684   **4.4. Exceeding natural thresholds in alpine areas**

685

686   The LDI-derived temperatures from LdRS exceeded the highest pre-industrial

687   temperatures in the early 1950s (Fig. 6c), under full anthropogenic influence. The

688   comparison between pre-industrial and post-industrial scenarios in the study site

689   highlights the human impact on natural trends. In this regard, the temperature increase

690   during the last stages of the LIA (from ~1690 to ~1850 CE), an analogue for a non-

691   anthropogenic temperature-increase scenario, was between ~1.2 and ~1.4°C

692   (~0.09°C/decade; Fig. 6), whereas the mean temperature rise throughout the 20th century

693 was ~1.8ºC (~0.18ºC/decade; Fig. 7). Both warming rates are roughly similar to those

694 reconstructed from MLR calibrations 1, 2, and 3: ~0.06-0.09ºC/decade for the last stages

695 of the LIA, and ~0.17-0.18ºC/decade for the 20th century. Although this means that on

696 average, the warming rate was two times faster throughout the 20th century than at the

697 end of the LIA (Fig. 7), these observations are based on a low sample density for the LIA

698 (8 samples), which might slightly increase the uncertainty for this period. By comparison,

699 average global temperatures rose by ~0.85ºC from 1880 to 2012 CE, corresponding to

700 0.06ºC/decade (IPCC, 2013), which highlight the high-elevation amplification effect of

701 temperatures on this vulnerable area.

702

703 Other European alpine areas in the Mediterranean region, such as those from the

704 Alps, experienced a slower warming rate during the 20th century (~0.11ºC/decade) (Fig.

705 7) (Auer et al., 2007; Böhm et al., 2010). This is ~1.6 times slower than the warming rate

706 recorded in the Sierra Nevada. This evidence, along with the generally smaller amount of

707 precipitation in the alpine areas of the western Mediterranean region (Auer et al., 2007;

708 Rodrigo et al., 1999), allows us to conclude that the 20th century environmental stress in

709 this area was greater than in the Alps.

710

711 Future scenarios are not optimistic for Sierra Nevada since temperatures at ~1000

712 masl may rise between 2.2ºC and 5.3ºC by the end of the 21st century (Pérez-Luque et al.,

713 2016), exceeding the global projections of the IPCC-2013 report (IPCC, 2013). However,

714 temperature projection and its subsequent impact on alpines areas of the Sierra Nevada

715 have not been satisfactorily assessed so far due to the lack of long-term quantitative

716 climatic records at these elevations (e.g., temperature). The LCD-based temperatures at

717 ~3000 masl will solve this lack of quantitative data and will be valuable to project future

718 scenarios in these alpine ecosystems where endemic and endangered species inhabit

719 (Blanca, 2001; Munguira and Martin, 1993).

720

721 **4.5. Impact on the southwesternmost European alpine glaciers**

722

723   The studied alpine area supported the southernmost glaciers in Europe during the

724 LIA. Glaciers and permanent snow fields below ~3000 masl, such as those of Corral del

725 Mulhacen (~2950 masl) whose last mention in the literature was between 1809 and 1849

726 CE (Oliva and Gomez-Ortiz, 2012), would have totally disappeared by the decrease in

727 regional precipitation during the first half of the 19th century (Rodrigo et al., 1999). The

728 climatic features at the end of the 19th century and the beginning of the 20th century did

729 not allow this glacier to re-establish itself (Fig. 8). Post-LIA climatic conditions have also

730 been proposed as the trigger for the melting of the Corral del Veleta Glacier in Sierra

731 Nevada (~3100 masl) at the beginning of the 20th century (Garcia-Alix et al., 2017; Oliva

732 and Gomez-Ortiz, 2012; Oliva et al., 2018). However, the LCDs in LdRS records show

733 that derived-temperatures did not exceed the levels of the 1850s until the late 1940s CE.

734 Precipitation was low in the southern Iberian Peninsula during the first half of the 20th

735 century, but similar, and even lower, precipitation values were registered before ~1850

736 CE (Rodrigo et al., 1999; Spanish National Weather Agency - AEMet Open Data, 2019)

737 (Fig. 8). Therefore, how could the glacier have retreated under this almost steady-state

738 scenario? A similar paradox has been described in the Alps (Painter et al., 2013), where

739 glaciers began to sharply retreat after the mid-19th century, even though temperature and

740 precipitation records would suggest that glacier expansion should have occurred at least

741 until the first decades of the 20th century. In this case, one of the proposed triggers for the

742 glacier retreat was the industrial black carbon deposition that amplified the solar radiation

743 absorbed at the snow surface and caused its subsequent melting - not a temperature or

744 precipitation change (Painter et al., 2013). Precipitation data from the southern Iberia

745 (Rodrigo et al., 1999) along with the LCD-reconstructed temperatures in LdRS records

746 suggest that temperature and precipitation were not the only drivers of glacial retreat that

747 led to the melting of permanent glaciers in the Sierra Nevada in the 1920s. Instead,

748 mirroring the case of the Alps, it is plausible that other factors reducing the albedo, such

749 as enhanced atmospheric deposition may have played a strong role. In this regard,

750 important atmospheric depositional events have been recorded in the study alpine sites of

751 southern Iberia from the mid-19th century to the first decades of the 20th century caused

752 by both enhanced North African dust fluxes (Mulitza et al., 2010) (Jiménez et al., 2018)

753 as well as a spike in atmospheric pollution (as observed in anthropogenic Pb and Hg

754 records in Sierra Nevada; Fig. 8) (Garcia-Alix et al., 2017; Garcia-Alix et al., 2013).

755 Similarly, both phenomena have been demonstrated as triggers for glacier retreat (Painter

756 et al., 2013) and snow melt in the Alps (Di Mauro et al., 2018).

757

758   Melting of the last glaciated area in the Sierra Nevada during the first decades of

759 the 20st century (Grunewald and Scheithauer, 2010) represents an important turning point

760 regarding recent environmental change in this alpine region (Garcia-Alix et al., 2017;

761 Jiménez et al., 2019). The rapid pace of environmental change in the area after this date

762 is attributed to an amplified effect of warming and aridification (Fig. 8b,c) that increased

763 stress on vulnerable ecosystems (Garcia-Alix et al., 2017; Jiménez et al., 2019; Jiménez

764 et al., 2018) with little hope for return of local glaciers.

765

766 **5. Concluding remarks**

767

This study shows the vulnerability of alpine regions and the importance of their monitoring for a better understanding of climate variability and future rapid responses. In this regard, algal-derived biomarkers from LdRS records have given rise to the first long-chain alky diol temperature calibration in freshwater environments by means of the comparison with instrumental temperature time-series. The combination of both short and long sediment cores has provided both a highly accurate LCD-temperature calibration for the instrumental period and a long-term historical perspective on the modern warming. This approach delivers a better time-integrated temperature model than discrete temperature measurements for the 20th century. Nevertheless, the lack of information about the biological sources of LCDs in the Sierra Nevada means that this calibration can only be potentially applied to other lakes with a similar LCD distribution or in the same alpine area.

The low sample resolution in the longer core before ~1500 CE precludes us from totally constraining the main natural controls on temperatures in this high-elevation site for the Common Era. However, the general trends support that the presumed primary effect of greenhouse gases on temperatures reconstructed from algal-lipids in this alpine region of southern Iberia is likely modulated by long-term solar forcing. In recent times, greenhouse gases seem to be the major temperature driver in this high elevation site. Volcanic forcing appears to have little effect on reconstructed temperatures in this alpine area. The Atlantic Multidecadal Oscillation (AMO) have also shown to have a long-term effect in the study area; however, due its complex nature, the real effect of the AMO on LCD-reconstructed temperatures in LdRS records cannot be fully constrained. In any case, the effect of the internal climate variability on local temperatures cannot be ruled out. LdRS records also highlight the potential impact that non-climatic environmental

793   drivers such as atmospheric dust and pollution deposition can have exerted on these

794   remote alpine environments (e.g., glacier melting).

795

796   Alpine temperatures of southern Iberia exceeded the highest scores reached during

797   pre-industrial times in the 1950s. This means that the rate of warming throughout the 20th

798   century doubled that of the last stages of the LIA. Furthermore, this modern warming rate

799   is even higher in the Sierra Nevada than in the Alps, pointing towards more environmental

800   stress in the Sierra Nevada ecosystems. In addition to the amplified effect of warming

801   and aridification, the local environmental pressure may have enhanced throughout the

802   20th century due to the disappearance of perennial snow fields and the gradual reduction

803   of the seasonal snow cover affecting the local water availability. This fragile alpine

804   environment will suffer severe consequences if the warming rates continue to be so high

805   or even higher as predicted by the end of the 21st century.

806

807   **Data availability.** Fractional abundances of the C_{28} 1,13-diol, C_{28} 1,14-diol, C_{30} 1,13-

808   diol, C_{30} 1,14-diol, C_{30} 1,15-diol, and C_{32} 1,15-diol from the studied cores (LdRS shc and

809   LdRS lgc) are available in Table S14, along with the four reference temperature time-

810   series at 3020 masl from 1908 to 2008.

811

812   **Supplement.** The supplement related to this article is available online at:

813   *https://doi.org/*

814

815   **Author contributions.** The study was conceived by AG-A and JLT. CPM, LJ, GJM,

816   and RSA recovered the sediment cores. AG-A analysed the samples and processed the

817 data. All co-authors discussed the data and equally contributed to the preparation of the

818 manuscript.

819

820 **Competing interests.** The authors declare that they have no conflict of interest.

821

822 **Acknowledgements.** We would like to thank to V. Slaymark (University of Glasgow),

823 for her help preparing and analysing the organic and inorganic samples, as well as F.J.

824 Bonet García, C. González Hidalgo, and M.J. Esteban Parra for providing the temperature

825 time-series from Sierra Nevada and South of Spain.

826

827 **Financial support.** This study was supported by the project P11-RNM 7332 of the "Junta

828 de Andalucía", the projects CGL2017-85415-R, CGL2013-47038-R and CGL2011-

829 23483 of the "Ministerio de Economía y Competitividad of Spain and Fondo Europeo de

830 Desarrollo Regional FEDER", the project 87/2007 of the OAPN-Ministerio de Medio

831 Ambiente, as well as the research group RNM-190 (Junta de Andalucía). A.G.-A. was

832 also supported by a Marie Curie Intra-European Fellowship of the 7th Framework

833 Programme for Research, Technological Development and Demonstration of the

834 European Commission (NAOSIPUK. Grant Number: PIEF-GA-2012-623027) and by a

835 Ramón y Cajal Fellowship RYC-2015-18966 of the Spanish Government (Ministerio de

836 Economía y Competividad). J.L.T. hosted the NAOSIPUK project (PIEF-GA-2012-

837 623027) at the University of Glasgow.

838

839 **References**

840

841 Abrantes, F., Lebreiro, S., Rodrigues, T., Gil, I., Bartels-Jónsdóttir, H., Oliveira, P.,

842   Kissel, C., and Grimalt, J. O.: Shallow-marine sediment cores record climate

843 variability and earthquake activity off Lisbon (Portugal) for the last 2000 years,

844 Quaternary Science Reviews, 24, 2477-2494, 2005.

845 Ammann, C. M., Joos, F., Schimel, D. S., Otto-Bliesner, B. L., and Tomas, R. A.: Solar

846 influence on climate during the past millennium: Results from transient

847 simulations with the NCAR Climate System Model, Proceedings of the National

848 Academy of Sciences, 104, 3713-3718, 2007.

849 Anderson, R. S., Jiménez-Moreno, G., Carrión, J., and Pérez-Martinez, C.: Postglacial

850 history of alpine vegetation, fire, and climate from Laguna de Río Seco, Sierra

851 Nevada, southern Spain, Quaternary Science Reviews, 30, 1615–1629, 2011.

852 Auer, I., Böhm, R., Jurkovic, A., Lipa, W., Orlik, A., Potzmann, R., Schöner, W.,

853 Ungersböck, M., Matulla, C., Briffa, K., Jones, P., Efthymiadis, D., Brunetti, M.,

854 Nanni, T., Maugeri, M., Mercalli, L., Mestre, O., Moisselin, J.-M., Begert, M.,

855 Müller-Westermeier, G., Kveton, V., Bochnicek, O., Stastny, P., Lapin, M.,

856 Szalai, S., Szentimrey, T., Cegnar, T., Dolinar, M., Gajic-Capka, M., Zaninovic,

857 K., Majstorovic, Z., and Nieplova, E.: HISTALP—historical instrumental

858 climatological surface time series of the Greater Alpine Region, International

859 Journal of Climatology, 27, 17-46, 2007.

860 Balzano, S., Lattaud, J., Villanueva, L., Rampen, S. W., Brussaard, C. P. D., van

861 Bleijswijk, J., Bale, N., Sinninghe Damsté, J. S., and Schouten, S.: A quest for the

862 biological sources of long chain alkyl diols in the western tropical North Atlantic

863 Ocean, Biogeosciences, 15, 5951-5968, 2018.

864 Barea-Arco, J., Pérez-Martínez, C., and Morales-Baquero, R.: Evidence of a mutualistic

865 relationship between an algal epibiont and its host, Daphnia pulicaria, Limnology

866 and Oceanography, 46, 871-881, 2001.

867 Blanca, G.: Flora amenazada y endémica de Sierra Nevada, Consejería de Medio

868 Ambiente de la Junta de Andalucía and University of Granada, 2001.

869 Böhm, R., Jones, P. D., Hiebl, J., Frank, D., Brunetti, M., and Maugeri, M.: The early

870 instrumental warm-bias: a solution for long central European temperature series

871 1760–2007, Climatic Change, 101, 41-67, 2010.

872 Büntgen, U., Krusic, P. J., Verstege, A., Sangüesa-Barreda, G., Wagner, S., Camarero,

873 J. J., Ljungqvist, F. C., Zorita, E., Oppenheimer, C., Konter, O., Tegel, W.,

874 Gärtner, H., Cherubini, P., Reinig, F., and Esper, J.: New Tree-Ring Evidence

875 from the Pyrenees Reveals Western Mediterranean Climate Variability since

876 Medieval Times, Journal of Climate, 30, 5295-5318, 2017.

877   Carrillo, P., Cruz-Pizarro, L., and Sánchez Castillo, P. M.: Aportación al conocimiento

878   del ciclo biológico de Chromulina nevadensis, Acta Botánica Malacitana, 16, 19-

879   26, 1991.

880   Castañeda, I. S. and Schouten, S.: A review of molecular organic proxies for examining

881   modern and ancient lacustrine environments, Quaternary Science Reviews, 30,

882   2851-2891, 2011.

883   Castillo Martín, A.: Lagunas de Sierra Nevada, Editorial Universidad de Granada,

884   Granada, 2009.

885   Catalan, J., Pla-Rabés, S., Wolfe, A. P., Smol, J. P., Rühland, K. M., Anderson, N. J.,

886   Kopáček, J., Stuchlík, E., Schmidt, R., Koinig, K. A., Camarero, L., Flower, R. J.,

887   Heiri, O., Kamenik, C., Korhola, A., Leavitt, P. R., Psenner, R., and Renberg, I.:

888   Global change revealed by palaeolimnological records from remote lakes: a

889   review, Journal of Paleolimnology, 49, 513-535, 2013.

890   Coddington, O., Lean, J. L., Pilewskie, P., Snow, M., and Lindholm, D.: A Solar

891   Irradiance Climate Data Record, Bulletin of the American Meteorological

892   Society, 97, 1265-1282, 2016.

893   Colcord, D. E., Cadieux, S. B., Brassell, S. C., Castañeda, I. S., Pratt, L. M., and White,

894   J. R.: Assessment of branched GDGTs as temperature proxies in sedimentary

895   records from several small lakes in southwestern Greenland, Organic

896   Geochemistry, 82, 33-41, 2015.

897   de Bar, M. W., Dorhout, D. J. C., Hopmans, E. C., Rampen, S. W., Sinninghe Damsté,

898   J. S., and Schouten, S.: Constraints on the application of long chain diol proxies in

899   the Iberian Atlantic margin, Organic Geochemistry, 101, 184-195, 2016.

900   Di Mauro, B., Garzonio, R., Rossini, M., Filippa, G., Pogliotti, P., Galvagno, M., Morra

901   di Cella, U., Migliavacca, M., Baccolo, G., Clemenza, M., Delmonte, B., Maggi,

902   V., Dumont, M., Tuzet, F., Lafaysse, M., Morin, S., Cremonese, E., and Colombo,

903   R.: Saharan dust events in the European Alps: role on snowmelt and geochemical

904   characterization, The Cryosphere Discuss., 2018, 1-28, 2018.

905   Easterling, D. R., Meehl, G. A., Parmesan, C., Changnon, S. A., Karl, T. R., and

906   Mearns, L. O.: Climate Extremes: Observations, Modeling, and Impacts, Science,

907   289, 2068-2074, 2000.

908   Foster, L. C., Pearson, E. J., Juggins, S., Hodgson, D. A., Saunders, K. M., Verleyen,

909   E., and Roberts, S. J.: Development of a regional glycerol dialkyl glycerol

910   tetraether (GDGT)–temperature calibration for Antarctic and sub-Antarctic lakes,
911   Earth and Planetary Science Letters, 433, 370-379, 2016.

912 Fyfe, J. C., Meehl, G. A., England, M. H., Mann, M. E., Santer, B. D., Flato, G. M.,
913   Hawkins, E., Gillett, N. P., Xie, S.-P., Kosaka, Y., and Swart, N. C.: Making
914   sense of the early-2000s warming slowdown, Nature Climate Change, 6, 224,
915   2016.

916 Gal, J.-K., Kim, J.-H., and Shin, K.-H.: Distribution of long chain alkyl diols along a
917   south-north transect of the northwestern Pacific region: Insights into a paleo sea
918   surface nutrient proxy, Organic Geochemistry, 119, 80-90, 2018.

919 García Montoro, C., Titos Martínez, M., and Casado Sánchez de Castilla, M.: Sierra
920   Nevada. Una expedición al pico de Veleta desde los Baños de Lanjarón (1859),
921   Universidad de Granada, Editorial Universidad de Granada, 2016.

922 Garcia-Alix, A., Jimenez Espejo, F. J., Toney, J. L., Jiménez-Moreno, G., Ramos-
923   Román, M. J., Anderson, R. S., Ruano, P., Queralt, I., Delgado Huertas, A., and
924   Kuroda, J.: Alpine bogs of southern Spain show human-induced environmental
925   change superimposed on long-term natural variations, Scientific Reports, 7, 7439
926   2017.

927 Garcia-Alix, A., Jimenez-Espejo, F. J., Lozano, J. A., Jimenez-Moreno, G., Martinez-
928   Ruiz, F., Garcia Sanjuan, L., Aranda Jimenez, G., Garcia Alfonso, E., Ruiz-
929   Puertas, G., and Anderson, R. S.: Anthropogenic impact and lead pollution
930   throughout the Holocene in Southern Iberia, Science of the Total Environment,
931   449, 451-460, 2013.

932 García-Alix, A., Jiménez-Moreno, G., Anderson, R. S., Jiménez Espejo, F. J., and
933   Delgado Huertas, A.: Holocene environmental change in southern Spain deduced
934   from the isotopic record of a high-elevation wetland in Sierra Nevada, Journal of
935   Paleolimnology, 48, 471-484, 2012.

936 Giorgi, F.: Climate change hot-spots, Geophysical Research Letters, 33, 2006.

937 Gómez-Navarro, J. J., Montávez, J. P., Jerez, S., Jiménez-Guerrero, P., Lorente-Plazas,
938   R., González-Rouco, J. F., and Zorita, E.: A regional climate simulation over the
939   Iberian Peninsula for the last millennium, Clim. Past, 7, 451-472, 2011.

940 Gómez-Navarro, J. J., Montávez, J. P., Jiménez-Guerrero, P., Jerez, S., Lorente-Plazas,
941   R., González-Rouco, J. F., and Zorita, E.: Internal and external variability in
942   regional simulations of the Iberian Peninsula climate over the last millennium,
943   Clim. Past, 8, 25-36, 2012.

944   Gonzalez-Hidalgo, J. C., Peña-Angulo, D., Brunetti, M., and Cortesi, N.: MOTEDAS: a
945   new monthly temperature database for mainland Spain and the trend in
946   temperature (1951–2010), International Journal of Climatology, 35, 4444-4463,
947   2015.

948   Grunewald, K. and Scheithauer, J.: Europe's southernmost glaciers: response and
949   adaptation to climate change, Journal of Glaciology, 56, 129-142, 2010.

950   Häkkinen, S., Rhines, P. B., and Worthen, D. L.: Atmospheric Blocking and Atlantic
951   Multidecadal Ocean Variability, Science, 334, 655-659, 2011.

952   Hansen, J., Ruedy, R., Sato, M., and Lo, K.: Global Surface Temperature Change,
953   Reviews of Geophysics, 48, 2010.

954   IPCC: Climate Change 2013: The Physical Science Basis. Contribution of Working
955   Group I to the Fifth Assessment Report of the Intergovernmental Panel on
956   Climate Change, Cambridge University Press, Cambridge, United Kingdom and
957   New York, NY, USA, 2013.

958   Jiménez, L., Conde-Porcuna, J. M., García-Alix, A., Toney, J. L., Anderson, R. S.,
959   Heiri, O., and Pérez-Martínez, C.: Ecosystem Responses to Climate-Related
960   Changes in a Mediterranean Alpine Environment Over the Last ~ 180 Years,
961   Ecosystems, 22, 563-577, 2019.

962   Jiménez, L., Romero-Viana, L., Conde-Porcuna, J. M., and Pérez-Martínez, C.:
963   Sedimentary photosynthetic pigments as indicators of climate and watershed
964   perturbations in an alpine lake in southern Spain, Limniteca, 34, 439-454, 2015.

965   Jiménez, L., Rühland, K. M., Jeziorski, A., Smol, J. P., and Pérez-Martínez, C.: Climate
966   change and Saharan dust drive recent cladoceran and primary production changes
967   in remote alpine lakes of Sierra Nevada, Spain, Global Change Biology, 28,
968   e139–e158, 2018.

969   Jiménez-Espejo, F. J., García-Alix, A., Jiménez-Moreno, G., Rodrigo-Gámiz, M.,
970   Anderson, R. S., Rodríguez-Tovar, F. J., Martínez-Ruiz, F., Giralt, S., Delgado
971   Huertas, A., and Pardo-Igúzquiza, E.: Saharan aeolian input and effective
972   humidity variations over western Europe during the Holocene from a high altitude
973   record, Chemical Geology, 374-375, 1-12, 2014.

974   Jiménez-Moreno, G. and Anderson, R. S.: Holocene vegetation and climate change
975   recorded in alpine bog sediments from the Borreguiles de la Virgen, Sierra
976   Nevada, southern Spain, Quaternary Research, 77, 44-53, 2012.

977   Jiménez-Moreno, G., García-Alix, A., Hernández-Corbalán, M. D., Anderson, R. S.,
978   and Delgado-Huertas, A.: Vegetation, fire, climate and human disturbance history
979   in the southwestern Mediterranean area during the late Holocene, Quaternary
980   Research, 79, 110-122, 2013.

981   Knudsen, M. F., Jacobsen, B. H., Seidenkrantz, M.-S., and Olsen, J.: Evidence for
982   external forcing of the Atlantic Multidecadal Oscillation since termination of the
983   Little Ice Age, Nature Communications, 5, 3323, 2014.

984   Lattaud, J., Dorhout, D., Schulz, H., Castañeda, I. S., Schefuß, E., Sinninghe Damsté, J.
985   S., and Schouten, S.: The C32 alkane-1,15-diol as a proxy of late Quaternary
986   riverine input in coastal margins, Clim. Past, 13, 1049-1061, 2017a.

987   Lattaud, J., Kim, J.-H., De Jonge, C., Zell, C., Sinninghe Damsté, J. S., and Schouten,
988   S.: The C32 alkane-1,15-diol as a tracer for riverine input in coastal seas,
989   Geochimica et Cosmochimica Acta, 202, 146-158, 2017b.

990   Lattaud, J., Kirkels, F., Peterse, F., Freymond, C. V., Eglinton, T. I., Hefter, J.,
991   Mollenhauer, G., Balzano, S., Villanueva, L., van der Meer, M. T. J., Hopmans,
992   E. C., Sinninghe Damsté, J. S., and Schouten, S.: Long-chain diols in rivers:
993   distribution and potential biological sources, Biogeosciences, 15, 4147-4161,
994   2018a.

995   Lattaud, J., Lo, L., Huang, J.-J., Chou, Y.-M., Gorbarenko, S. A., Sinninghe Damsté, J.
996   S., and Schouten, S.: A Comparison of Late Quaternary Organic Proxy-Based
997   Paleotemperature Records of the Central Sea of Okhotsk, Paleoceanography and
998   Paleoclimatology, 33, 732-744, 2018b.

999   Longo, W. M., Huang, Y., Yao, Y., Zhao, J., Giblin, A. E., Wang, X., Zech, R.,
1000   Haberzettl, T., Jardillier, L., Toney, J., Liu, Z., Krivonogov, S., Kolpakova, M.,
1001   Chu, G., D'Andrea, W. J., Harada, N., Nagashima, K., Sato, M., Yonenobu, H.,
1002   Yamada, K., Gotanda, K., and Shinozuka, Y.: Widespread occurrence of distinct
1003   alkenones from Group I haptophytes in freshwater lakes: Implications for
1004   paleotemperature and paleoenvironmental reconstructions, Earth and Planetary
1005   Science Letters, 492, 239-250, 2018.

1006   López-Moreno, J. I., Vicente-Serrano, S. M., Morán-Tejeda, E., Lorenzo-Lacruz, J.,
1007   Kenawy, A., and Beniston, M.: Effects of the North Atlantic Oscillation (NAO)
1008   on combined temperature and precipitation winter modes in the Mediterranean
1009   mountains: Observed relationships and projections for the 21st century, Global
1010   and Planetary Change, 77, 62-76, 2011.

1011   Luterbacher, J., Werner, J. P., Smerdon, J. E., Fernández-Donado, L., González-Rouco,
1012   F. J., Barriopedro, D., Ljungqvist, F. C., Büntgen, U., Zorita, E., Wagner, S.,
1013   Esper, J., McCarroll, D., Toreti, A., Frank, D., Jungclaus, J. H., Barriendos, M.,
1014   Bertolin, C., Bothe, O., Brázdil, R., Camuffo, D., Dobrovolný, P., Gagen, M.,
1015   García-Bustamante, E., Ge, Q., Gómez-Navarro, J. J., Guiot, J., Hao, Z., Hegerl,
1016   G. C., Holmgren, K., Klimenko, V. V., Martín-Chivelet, J., Pfister, C., Roberts,
1017   N., Schindler, A., Schurer, A., Solomina, O., von Gunten, L., Wahl, E., Wanner,
1018   H., Wetter, O., Xoplaki, E., Yuan, N., Zanchettin, D., Zhang, H., and Zerefos, C.:
1019   European summer temperatures since Roman times, Environmental Research
1020   Letters, 11, 024001, 2016.
1021   Mann, M. E., Zhang, Z., Rutherford, S., Bradley, R. S., Hughes, M. K., Shindell, D.,
1022   Ammann, C., Faluvegi, G., and Ni, F.: Global Signatures and Dynamical Origins
1023   of the Little Ice Age and Medieval Climate Anomaly, Science, 326, 1256-1260,
1024   2009.
1025   Marotzke, J. and Forster, P. M.: Forcing, feedback and internal variability in global
1026   temperature trends, Nature, 517, 565-570, 2015.
1027   Mather, T. A., Pyle, D. M., and Oppenheimer, C.: Tropospheric Volcanic Aerosol. In:
1028   Volcanism and the Earth's Atmosphere, American Geophysical Union, 2013.
1029   Médail, F. and Quézel, P.: Biodiversity Hotspots in the Mediterranean Basin: Setting
1030   Global Conservation Priorities, Conservation Biology, 13, 1510-1513, 1999.
1031   Mesa-Fernández, J. M., Jiménez-Moreno, G., Rodrigo-Gámiz, M., García-Alix, A.,
1032   Jiménez-Espejo, F. J., Martínez-Ruiz, F., Anderson, R. S., Camuera, J., and
1033   Ramos-Román, M. J.: Vegetation and geochemical responses to Holocene rapid
1034   climate change in the Sierra Nevada (southeastern Iberia): the Laguna Hondera
1035   record, Clim. Past, 14, 1687-1706, 2018.
1036   Morales-Baquero, R., Pulido-Villena, E., and Reche, I.: Atmospheric inputs of
1037   phosphorus and nitrogen to the southwest Mediterranean region: Biogeochemical
1038   responses of high mountain lakes, Limnology and Oceanography 51, 830–837,
1039   2006.
1040   Moreno, A., Pérez, A., Frigola, J., Nieto-Moreno, V., Rodrigo-Gámiz, M., Martrat, B.,
1041   González-Sampériz, P., Morellón, M., Martín-Puertas, C., Corella, J. P.,
1042   Belmonte, Á., Sancho, C., Cacho, I., Herrera, G., Canals, M., Grimalt, J. O.,
1043   Jiménez-Espejo, F., Martínez-Ruiz, F., Vegas-Vilarrúbia, T., and Valero-Garcés,

B. L.: The Medieval Climate Anomaly in the Iberian Peninsula reconstructed from marine and lake records, Quaternary Science Reviews, 43, 16-32, 2012.

Mulitza, S., Heslop, D., Pittauerova, D., Fischer, H. W., Meyer, I., Stuut, J.-B., Zabel, M., Mollenhauer, G., Collins, J. A., Kuhnert, H., and Schulz, M.: Increase in African dust flux at the onset of commercial agriculture in the Sahel region, Nature, 466, 226-228, 2010.

Munguira, M. L. and Martin, J.: The Sierra Nevada blue, Polyommatus golgus (Hiibner). In: Conservation Biology of Lycaenidae (Butterflies), New, T. R. (Ed.), IUCN, Gland, Switzerland, 1993.

Nieto-Moreno, V., Martínez-Ruiz, F., Willmott, V., García-Orellana, J., Masqué, P., and Sinninghe Damsté, J. S.: Climate conditions in the westernmost Mediterranean over the last two millennia: An integrated biomarker approach, Organic Geochemistry, 55, 1-10, 2013.

O'Reilly, C. H., Woollings, T., and Zanna, L.: The Dynamical Influence of the Atlantic Multidecadal Oscillation on Continental Climate, Journal of Climate, 30, 7213-7230, 2017.

Observatorio del cambio global de Sierra Nevada: Linaria v1.0. iEcolab – Laboratorio de Ecología Terrestre – Universidad de Granada, http://linaria.obsnev.es, 2016.

Oliva, M. and Gomez-Ortiz, A.: Late-Holocene environmental dynamics and climate variability in a Mediterranean high mountain environment (Sierra Nevada, Spain) inferred from lake sediments and historical sources, The Holocene, 22, 915-927, 2012.

Oliva, M., Ruiz-Fernández, J., Barriendos, M., Benito, G., Cuadrat, J. M., Domínguez-Castro, F., García-Ruiz, J. M., Giralt, S., Gómez-Ortiz, A., Hernández, A., López-Costas, O., López-Moreno, J. I., López-Sáez, J. A., Martínez-Cortizas, A., Moreno, A., Prohom, M., Saz, M. A., Serrano, E., Tejedor, E., Trigo, R., Valero-Garcés, B., and Vicente-Serrano, S. M.: The Little Ice Age in Iberian mountains, Earth-Science Reviews, 177, 175-208, 2018.

Painter, T. H., Flanner, M. G., Kaser, G., Marzeion, B., VanCuren, R. A., and Abdalati, W.: End of the Little Ice Age in the Alps forced by industrial black carbon, Proceedings of the National Academy of Sciences, 110, 15216-15221, 2013.

Pauli, H., Gottfried, M., Dullinger, S., Abdaladze, O., Akhalkatsi, M., Alonso, J. L. B., Coldea, G., Dick, J., Erschbamer, B., Calzado, R. F., Ghosn, D., Holten, J. I., Kanka, R., Kazakis, G., Kollár, J., Larsson, P., Moiseev, P., Moiseev, D., Molau,

1078   U., Mesa, J. M., Nagy, L., Pelino, G., Puşcaş, M., Rossi, G., Stanisci, A.,

1079   Syverhuset, A. O., Theurillat, J.-P., Tomaselli, M., Unterluggauer, P., Villar, L.,

1080   Vittoz, P., and Grabherr, G.: Recent Plant Diversity Changes on Europe's

1081   Mountain Summits, Science, 336, 353-355, 2012.

1082 Pérez-Luque, A., Pérez-Pérez, R., Aspizua, R., Muñoz, J., and Bonet, F.: Climate in

1083   Sierra Nevada: present and future. . In: Change impacts in Sierra Nevada:

1084   challenges for conservation, Zamora, R., Pérez-Luque, A., Bonet, F., Barea-

1085   Azcón, J., and Aspizua, R. (Eds.), Consejería de Medio Ambiente y Ordenación

1086   del Territorio, Junta de Andalucía, Andalucia, 2016.

1087 Pulido-Villena, E., Reche, I., and Morales-Baquero, R.: Food web reliance on

1088   allochthonous carbon in two high mountain lakes with contrasting catchments: a

1089   stable isotope approach, Canadian Journal of Fisheries and Aquatic Sciences, 62,

1090   2640–2648 2005.

1091 Ramos-Román, M. J., Jiménez-Moreno, G., R.S., A., García-Alix, A., Toney, J. L.,

1092   Jiménez-Espejo, F. J., and Carrión, J. S.: Centennial-scale vegetation and North

1093   Atlantic Oscillation changes during the Late Holocene in the southern Iberia,

1094   Quaternary Science Reviews, 143, 84-95, 2016.

1095 Rampen, S. W., Datema, M., Rodrigo-Gámiz, M., Schouten, S., Reichart, G.-J., and

1096   Sinninghe Damsté, J. S.: Sources and proxy potential of long chain alkyl diols in

1097   lacustrine environments, Geochimica et Cosmochimica Acta, 144, 59-71, 2014a.

1098 Rampen, S. W., Schouten, S., Koning, E., Brummer, G.-J. A., and Sinninghe Damsté, J.

1099   S.: A 90 kyr upwelling record from the northwestern Indian Ocean using a novel

1100   long-chain diol index, Earth and Planetary Science Letters, 276, 207-213, 2008.

1101 Rampen, S. W., Willmott, V., Kim, J.-H., Rodrigo-Gámiz, M., Uliana, E., Mollenhauer,

1102   G., Schefuß, E., Sinninghe Damsté, J. S., and Schouten, S.: Evaluation of long

1103   chain 1,14-alkyl diols in marine sediments as indicators for upwelling and

1104   temperature, Organic Geochemistry, 76, 39-47, 2014b.

1105 Rampen, S. W., Willmott, V., Kim, J.-H., Uliana, E., Mollenhauer, G., Schefuß, E.,

1106   Sinninghe Damsté, J. S., and Schouten, S.: Long chain 1,13- and 1,15-diols as a

1107   potential proxy for palaeotemperature reconstruction, Geochimica et

1108   Cosmochimica Acta, 84, 204-216, 2012.

1109 Reche, I., Ortega-Retuerta, E., Romera, O., Pulido-Villena, E., Morales-Baquero, R.,

1110   and Casamayor, E. O.: Effect of Saharan dust inputs on bacterial activity and

1111   community composition in Mediterranean lakes and reservoirs, Limnol.

1112   Oceanogr, 54, 869–879, 2009.

1113 Reimer, P. J., Bard, E., Bayliss, A., Beck, J. W., Blackwell, P. G., Ramsey, C. B., Buck,

1114   C. E., Cheng, H., Edwards, R. L., Friedrich, M., Grootes, P. M., Guilderson, T. P.,

1115   Haflidason, H., Hajdas, I., Hatté, C., Heaton, T. J., Hoffmann, D. L., Hogg, A. G.,

1116   Hughen, K. A., Kaiser, K. F., Kromer, B., Manning, S. W., Niu, M., Reimer, R.

1117   W., Richards, D. A., Scott, E. M., Southon, J. R., Staff, R. A., Turney, C. S. M.,

1118   and van der Plicht, J.: IntCal13 and Marine13 Radiocarbon Age Calibration

1119   Curves 0–50,000 Years cal BP, Radiocarbon, 55, 1869-1887, 2013.

1120 Rodrigo, F. S., Esteban-Parra, M. J., Pozo-Vázquez, D., and Castro-Díez, Y.: A 500-

1121   year precipitation record in Southern Spain, International Journal of Climatology,

1122   19, 1233-1253, 1999.

1123 Rodrigo-Gámiz, M., Martínez-Ruiz, F., Rampen, S. W., Schouten, S., and Sinninghe

1124   Damsté, J. S.: Sea surface temperature variations in the western Mediterranean

1125   Sea over the last 20 kyr: A dual-organic proxy (UK′ 37 and LDI) approach,

1126   Paleoceanography, 29, 87-98, 2014.

1127 Rodrigo-Gámiz, M., Rampen, S. W., de Haas, H., Baas, M., Schouten, S., and

1128   Sinninghe Damsté, J. S.: Constraints on the applicability of the organic

1129   temperature proxies UK'37, TEX86 and LDI in the subpolar region around

1130   Iceland, Biogeosciences, 12, 6573-6590, 2015.

1131 Romero-Viana, L., Kienel, U., and Sachse, D.: Lipid biomarker signatures in a

1132   hypersaline lake on Isabel Island (Eastern Pacific) as a proxy for past rainfall

1133   anomaly (1942–2006AD), Palaeogeography, Palaeoclimatology, Palaeoecology,

1134   350-352, 49-61, 2012.

1135 Sánchez-Castillo, P. M.: Algas de las lagunas de alta montaña de Sierra Nevada

1136   (Granada, España), Acta Botánica Malacitana, 13, 21 -52, 1988.

1137 Sánchez-López, G., Hernández, A., Pla-Rabes, S., Trigo, R. M., Toro, M., Granados, I.,

1138   Sáez, A., Masqué, P., Pueyo, J. J., Rubio-Inglés, M. J., and Giralt, S.: Climate

1139   reconstruction for the last two millennia in central Iberia: The role of East Atlantic

1140   (EA), North Atlantic Oscillation (NAO) and their interplay over the Iberian

1141   Peninsula, Quaternary Science Reviews, 149, 135-150, 2016.

1142 Schmidt, G. A., Jungclaus, J. H., Ammann, C. M., Bard, E., Braconnot, P., Crowley, T.

1143   J., Delaygue, G., Joos, F., Krivova, N. A., Muscheler, R., Otto-Bliesner, B. L.,

1144   Pongratz, J., Shindell, D. T., Solanki, S. K., Steinhilber, F., and Vieira, L. E. A.:

1145   Climate forcing reconstructions for use in PMIP simulations of the last

1146   millennium (v1.0), Geosci. Model Dev., 4, 33-45, 2011.

1147 Schröter, D., Cramer, W., Leemans, R., Prentice, I. C., Araújo, M. B., Arnell, N. W.,

1148   Bondeau, A., Bugmann, H., Carter, T. R., Gracia, C. A., de la Vega-Leinert, A.

1149   C., Erhard, M., Ewert, F., Glendining, M., House, J. I., Kankaanpää, S., Klein, R.

1150   J. T., Lavorel, S., Lindner, M., Metzger, M. J., Meyer, J., Mitchell, T. D.,

1151   Reginster, I., Rounsevell, M., Sabaté, S., Sitch, S., Smith, B., Smith, J., Smith, P.,

1152   Sykes, M. T., Thonicke, K., Thuiller, W., Tuck, G., Zaehle, S., and Zierl, B.:

1153   Ecosystem Service Supply and Vulnerability to Global Change in Europe,

1154   Science, 310, 1333-1337, 2005.

1155 Shimokawara, M., Nishimura, M., Matsuda, T., Akiyama, N., and Kawai, T.: Bound

1156   forms, compositional features, major sources and diagenesis of long chain, alkyl

1157   mid-chain diols in Lake Baikal sediments over the past 28,000 years, Organic

1158   Geochemistry, 41, 753-766, 2010.

1159 Sicre, M.-A., Jalali, B., Martrat, B., Schmidt, S., Bassetti, M.-A., and Kallel, N.: Sea

1160   surface temperature variability in the North Western Mediterranean Sea (Gulf of

1161   Lion) during the Common Era, Earth and Planetary Science Letters, 456, 124-133,

1162   2016.

1163 Sigl, M., Winstrup, M., McConnell, J. R., Welten, K. C., Plunkett, G., Ludlow, F.,

1164   Buntgen, U., Caffee, M., Chellman, N., Dahl-Jensen, D., Fischer, H., Kipfstuhl,

1165   S., Kostick, C., Maselli, O. J., Mekhaldi, F., Mulvaney, R., Muscheler, R.,

1166   Pasteris, D. R., Pilcher, J. R., Salzer, M., Schupbach, S., Steffensen, J. P., Vinther,

1167   B. M., and Woodruff, T. E.: Timing and climate forcing of volcanic eruptions for

1168   the past 2,500 years, Nature, 523, 543-549, 2015.

1169 Sinninghe Damsté, J. S., Rampen, S., Irene, W., Rijpstra, C., Abbas, B., Muyzer, G.,

1170   and Schouten, S.: A diatomaceous origin for long-chain diols and mid-chain

1171   hydroxy methyl alkanoates widely occurring in quaternary marine sediments:

1172   indicators for high-nutrient conditions, Geochimica et Cosmochimica Acta, 67,

1173   1339-1348, 2003.

1174 Smith, M., De Deckker, P., Rogers, J., Brocks, J., Hope, J., Schmidt, S., Lopes dos

1175   Santos, R., and Schouten, S.: Comparison of $U37K'$, TEX86H and LDI

1176   temperature proxies for reconstruction of south-east Australian ocean

1177   temperatures, Organic Geochemistry, 64, 94-104, 2013.

1178 Spanish National Weather Agency - AEMet Open Data: AEMet Open Data.

1179   http://www.aemet.es/es/datos_abiertos/AEMET_OpenData, 2019.

1180 Steinhilber, F., Beer, J., and Fröhlich, C.: Total solar irradiance during the Holocene,

1181   Geophysical Research Letters, 36, 2009.

1182 Stuiver, M. and Quay, P. D.: Changes in Atmospheric Carbon-14 Attributed to a

1183   Variable Sun, Science, 207, 11-19, 1980.

1184 Tejedor, E., Saz, M. Á., Cuadrat, J. M., Esper, J., and de Luis, M.: Temperature

1185   variability in the Iberian Range since 1602 inferred from tree-ring records, Clim.

1186   Past, 13, 93-105, 2017.

1187 Theroux, S., D'Andrea, W. J., Toney, J., Amaral-Zettler, L., and Huang, Y.:

1188   Phylogenetic diversity and evolutionary relatedness of alkenone-producing

1189   haptophyte algae in lakes: Implications for continental paleotemperature

1190   reconstructions, Earth and Planetary Science Letters, 300, 311-320, 2010.

1191 Titos Martínez, M.: Los trabajos de desagüe de las lagunas de Sierra Nevada: un largo

1192   despropósito medioambiental, Revista del Centro de Estudios Históricos de

1193   Granada y su Reino, 2019. 223-243, 2019.

1194 Titos Martínez, M. and Ramos Lafuente, A. J.: El refugio más antiguo de Sierra

1195   Nevada: Construido en 1891, aún se mantiene en pie, Andalucía en la historia,

1196   2016. 48-53, 2016.

1197 Trouet, V., Esper, J., Graham, N. E., Baker, A., Scourse, J. D., and Frank, D. C.:

1198   Persistent Positive North Atlantic Oscillation Mode Dominated the Medieval

1199   Climate Anomaly, Science, 324, 78-80, 2009.

1200 Versteegh, G. J. M., Bosch, H. J., and De Leeuw, J. W.: Potential palaeoenvironmental

1201   information of C24 to C36 mid-chain diols, keto-ols and mid-chain hydroxy fatty

1202   acids; a critical review, Organic Geochemistry, 27, 1-13, 1997.

1203 Villanueva, L., Besseling, M., Rodrigo-Gámiz, M., Rampen, S. W., Verschuren, D., and

1204   Sinninghe Damsté, J. S.: Potential biological sources of long chain alkyl diols in a

1205   lacustrine system, Organic Geochemistry, 68, 27-30, 2014.

1206 Volkman, J. K., Barrett, S. M., and Blackburn, S. I.: Eustigmatophyte microalgae are

1207   potential sources of C29 sterols, C22–C28 n-alcohols and C28–C32 n-alkyl diols

1208   in freshwater environments, Organic Geochemistry, 30, 307-318, 1999.

1209 Waters, C. N., Zalasiewicz, J., Summerhayes, C., Barnosky, A. D., Poirier, C.,

1210   Gałuszka, A., Cearreta, A., Edgeworth, M., Ellis, E. C., Ellis, M., Jeandel, C.,

1211   Leinfelder, R., McNeill, J. R., Richter, D. d., Steffen, W., Syvitski, J., Vidas, D.,

1212   Wagreich, M., Williams, M., Zhisheng, A., Grinevald, J., Odada, E., Oreskes, N.,
1213   and Wolfe, A. P.: The Anthropocene is functionally and stratigraphically distinct
1214   from the Holocene, Science, 351, 2016.

1215   Willmott, V., Rampen, S. W., Domack, E., Canals, M., Sinninghe Damsté, J. S., and
1216   Schouten, S.: Holocene changes in Proboscia diatom productivity in shelf waters
1217   of the north-western Antarctic Peninsula, Antarctic Science, 22, 3-10, 2010.

1218   Yu, M., Zhang, H., Li, L., and Zhao, M.: Spatial Distributions and Potential Sources of
1219   Long Chain (C30, C32 1,15-) Alkyl Diols in Surface Sediments from Eastern
1220   China Marginal Seas, Journal of Ocean University of China, 17, 1114-1122, 2018.
1221

1222   **FIGURES**
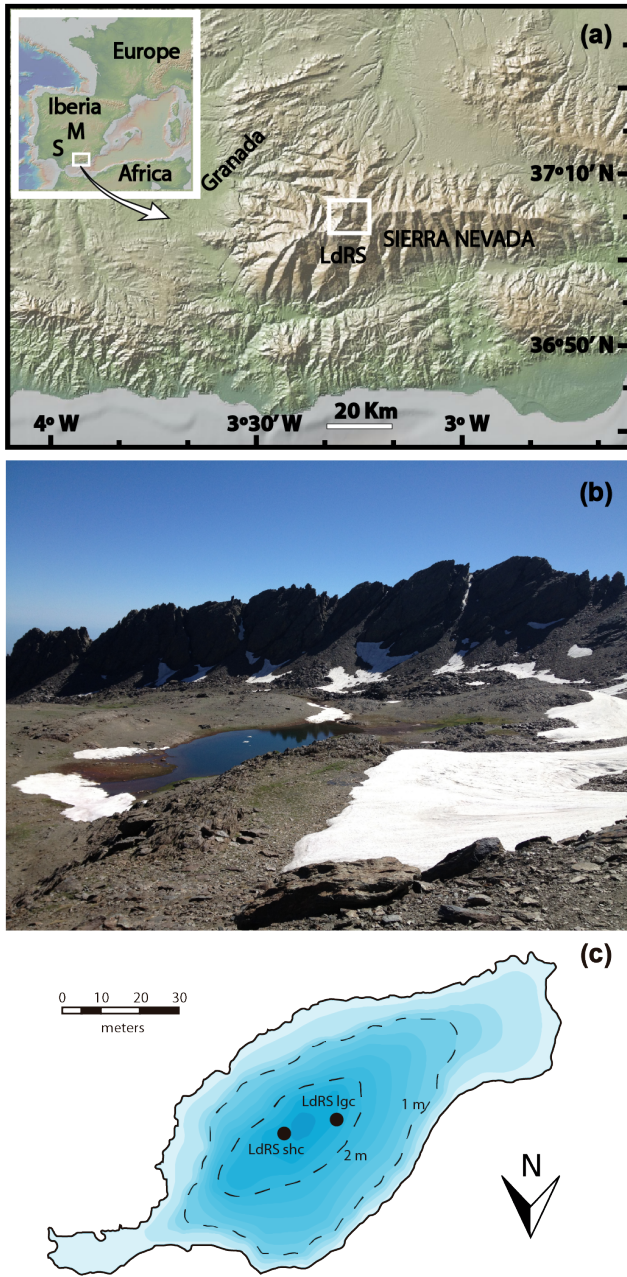
1223

1224   **Figure 1. Geographical setting.** (**a**) Location of the Sierra Nevada in the western

1225   Mediterranean region, Madrid (M), Sevilla (S) and Granada observatories, as well as the

1226   studied area: Laguna de Río Seco (LdRS), (**b**) LdRS catchment basin (0.42 ha) in spring

1227   2013, (**c**) bathymetry map of LdRS along with the sampling points of both cores. Data

1228   source and software: (**a**) map created by A. García-Alix using GeoMapApp (3.6.6)

1229   (http://www.geomapapp.org), (**b**) picture from A. García-Alix, (**c**) digitalized map of a

1230   bathymetry report from Egmasa S.A.
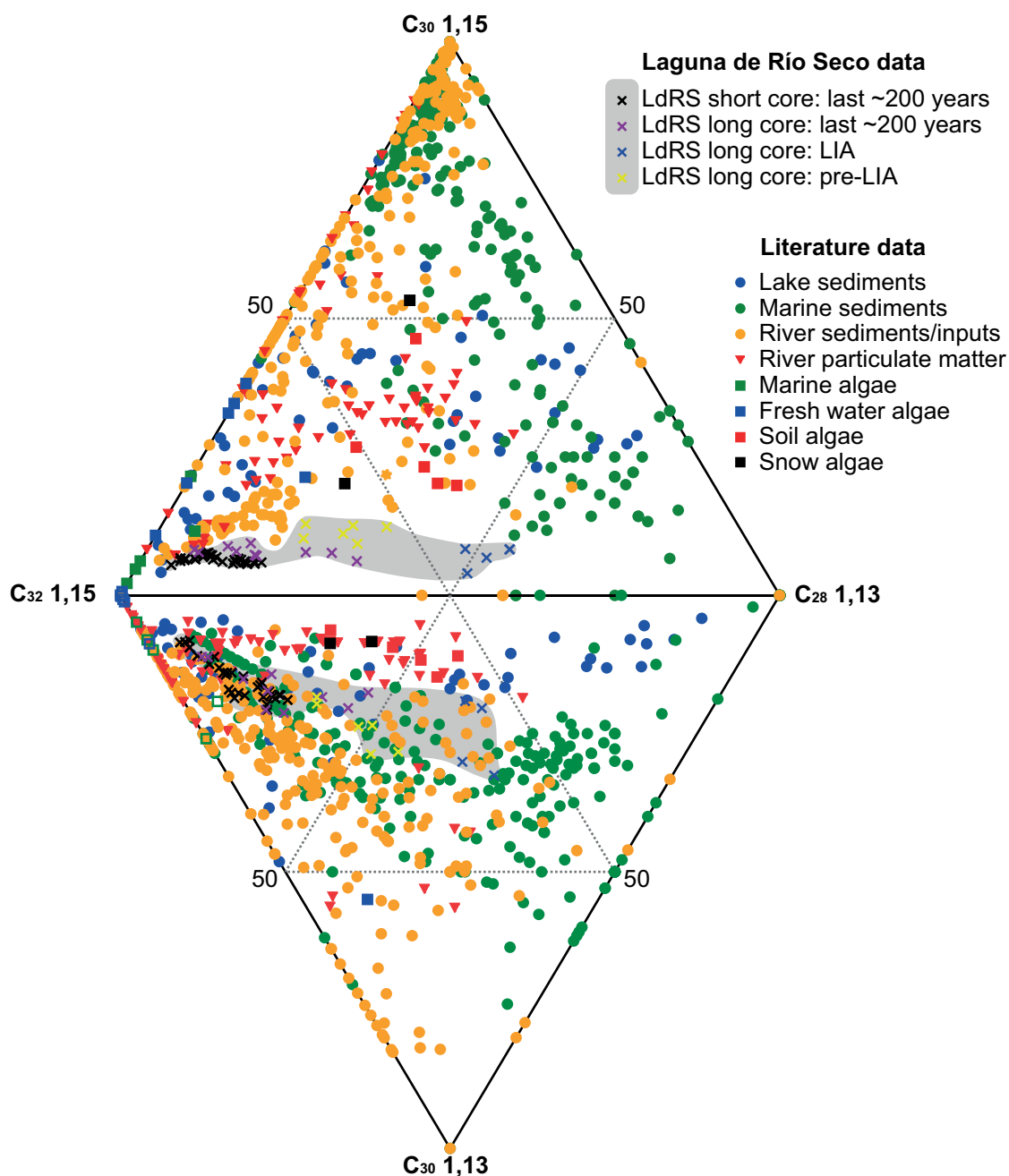
1231

Figure 2. Double-ternary diagram of the relative abundances of C_{28} 1,13-diol, C_{30} 1,13-diol, C_{30} 1,15-diol, and C_{32} 1,15-diol from LdRS short core (LdRS shc ~200 years) and LdRS long core (LdRS lgc ~1500 years). Diol data compiled from the literature: lake sediments (Rampen et al., 2014a), algal cultures (Rampen et al., 2014a), marine sediments (de Bar et al., 2016; Lattaud et al., 2017a; Rampen et al., 2014b; Rampen et al., 2012), river sediments/inputs (de Bar et al., 2016; Lattaud et al., 2017b), river particulate organic matter (Lattaud et al., 2018a).
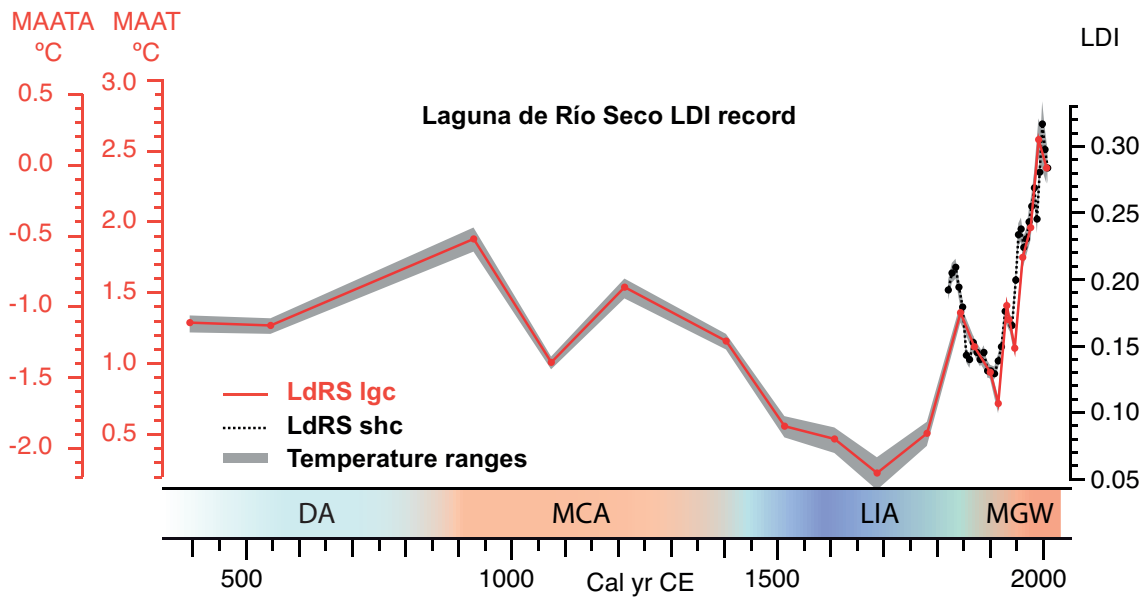
Figure 3. LDI record from LdRS, including both long core (solid line) and short core (dashed line), mean annual air temperature (MAAT ºC) reconstruction from LDI records of LdRS, as well as mean annual air temperature anomaly reconstruction (MAATAºC) respect to the annual MAAT of the last 30 years (1979-2008). The grey shade shows the reconstructed maximum and minimum temperature ranges obtained from the four LDI individual calibrations.
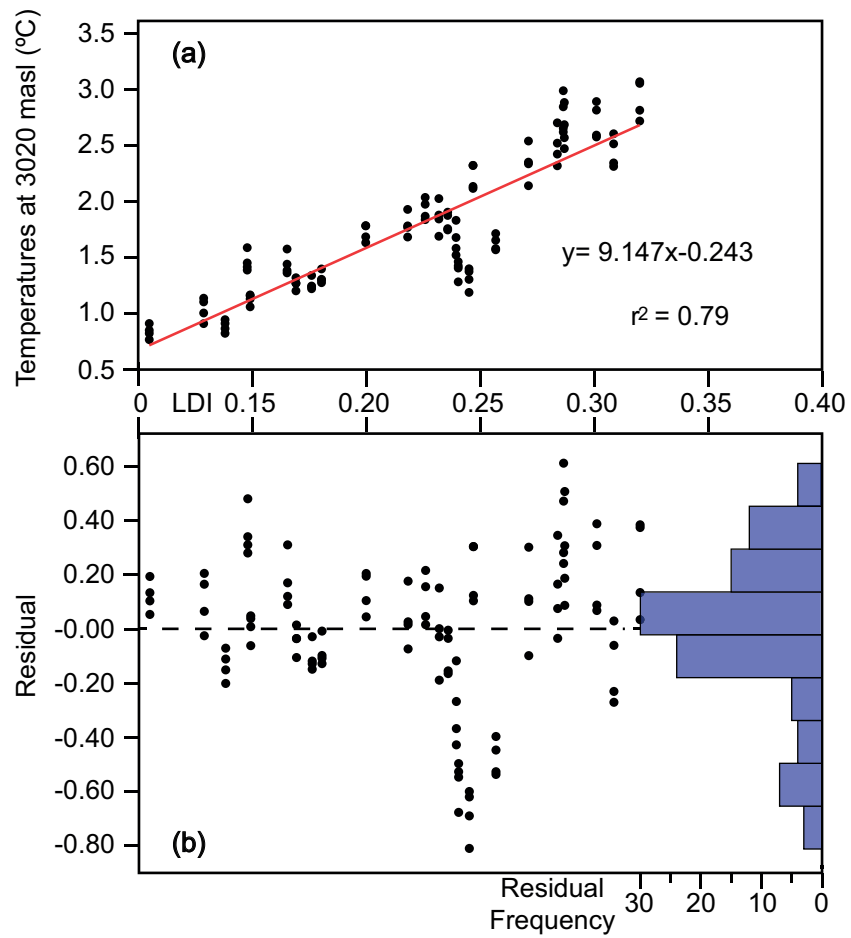
1246
1247
1248 **Figure 4. LDI temperature calibration**. **(a)** Correlations by means of ordinary least

1249 square regression between the both LDI records from LdRS (from 1908 to 2008) and the

1250 four reference temperature time-series at 3020 masl. **(b)** LDI values of LdRS *vs* residual

1251 temperatures (calculated between the calibrated LDI temperatures *vs* reference

1252 temperature time series at 3020 masl), as well as the histogram of the frequency of these

1253 residuals.
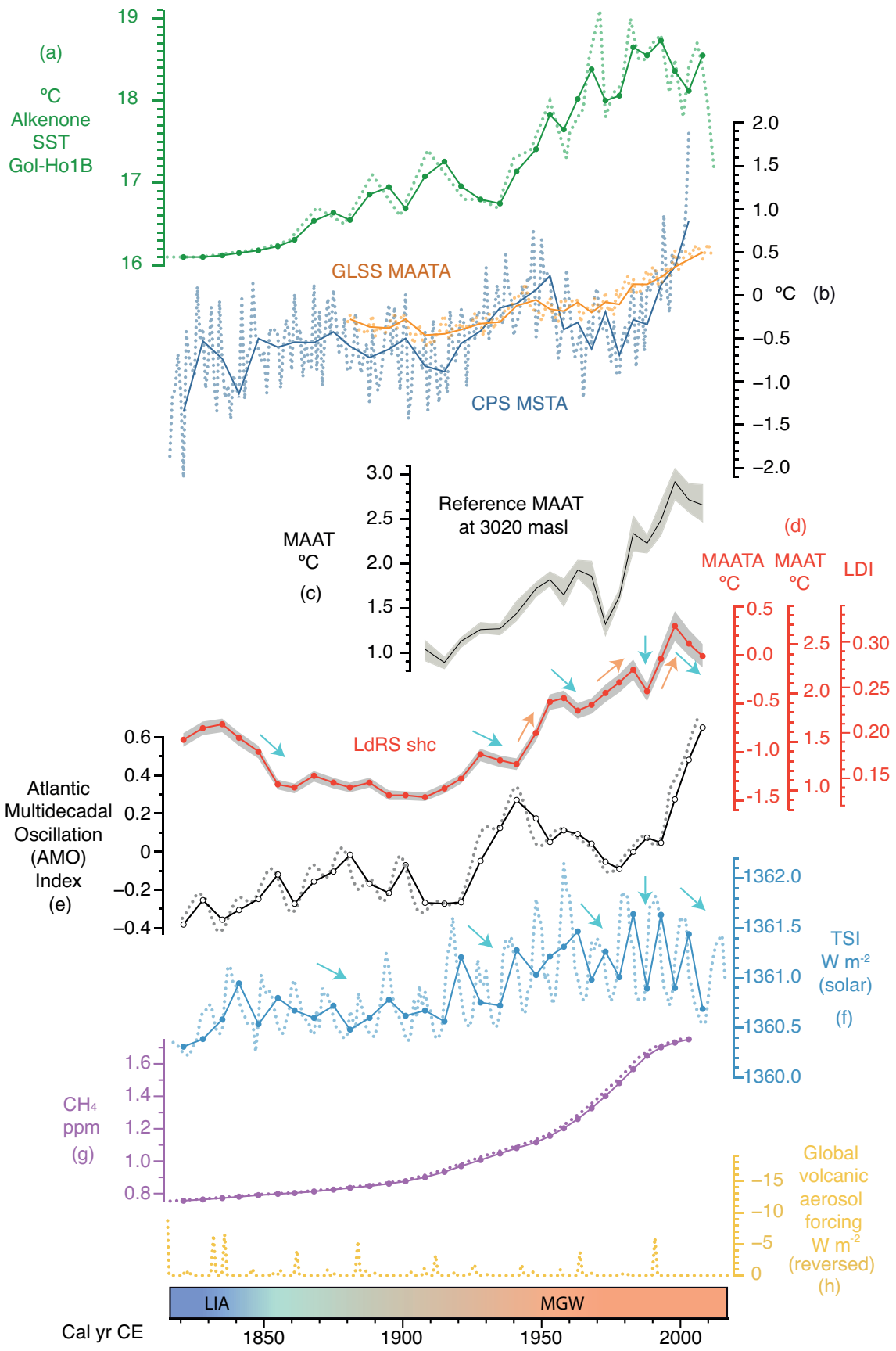
Figure 5. Comparison of the LDI record and the reconstructed temperatures for the last ~200 years of LdRS with marine and terrestrial temperature records, Atlantic multidecadal oscillations, greenhouse gases, solar radiation and volcanic eruption records. Original data are in dashed lines. Solid lines represent the same time averaging as the LDI data in LdRS shc (data were linearly interpolated and time-averaged to the same resolution as the sampling points of LdRS shc) to facilitate the correlation. **(a)** Alkenone-derived Sea Surface Temperatures (SST, ºC) of the core Gol-Ho1B_KSGC-31 (Gulf of Lion: NW Mediterranean Sea (Sicre et al., 2016)), **(b)** Composite-plus-scaling (CPS) mean summer temperature anomaly reconstruction from tree rings records in Europe with respect to 1974-2003 (MSTA ºC) (Luterbacher et al., 2016) as well as global land and sea surface (GLSS) mean annual temperature anomalies with respect to 1979-2008 CE (MAATA ºC) (Hansen et al., 2010), (c) Summary of the four reference temperature time-series at 3020 masl: grey shade show the maximum and minimum temperature range and the black solid line represent the mean temperature values, **(d)** LDI record along with reconstructed mean annual air temperatures (MAAT ºC) and mean annual air temperature anomalies with respect to 1979-2008 CE (MAATA ºC) for the last ~200 years in LdRS, **(e)** Atlantic Multidecadal Oscillation (AMO) reconstruction (Mann et al., 2009), **(f)** high resolution total solar irradiance reconstruction (TSI, W m^{-2}) (Coddington et al., 2016), **(g)** reconstructed concentration of atmospheric CH_4 (ppm) (Schmidt et al., 2011), and **(h)** reconstruction of the global volcanic aerosol forcing (W m^{-2}) (reversed) (Sigl et al., 2015). Acronyms: LIA, Little Ice Age; MGW, Modern Global Warming. Blue arrows: decrease; orange arrows: increase.
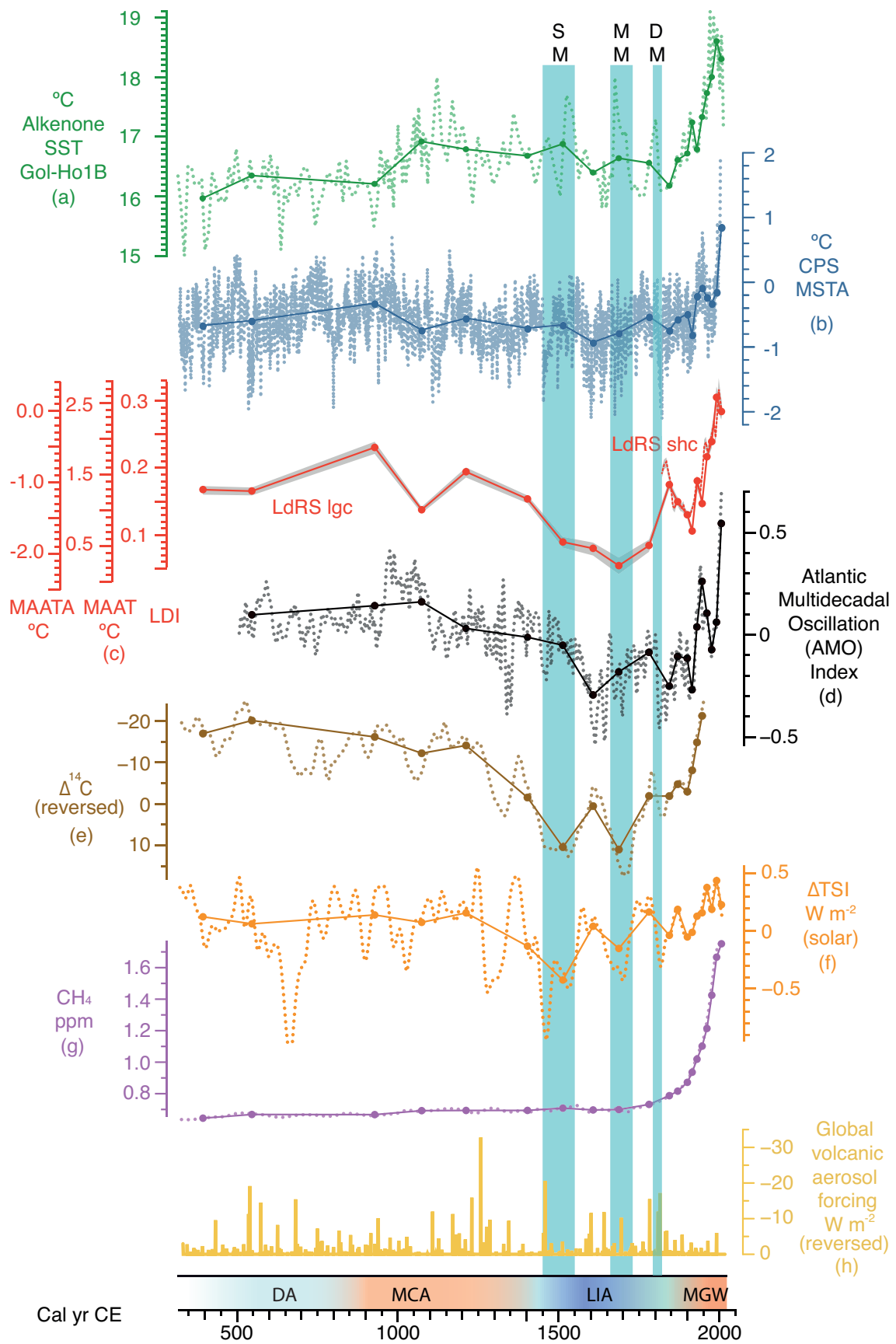
1278 **Figure 6.** **Comparison of the LDI record and the reconstructed temperatures for the**

1279 **last ~1500 years of LdRS with marine and terrestrial temperature records, Atlantic**

1280 **multidecadal oscillations, solar radiation, greenhouse gases, and volcanic eruption**

1281 **records.** Original data are in dashed lines. Solid dots represent the same time averaging

1282 as the LDI data in LdRS lgc (data were linearly interpolated and time-averaged to the

1283 same resolution as the sampling points of LdRS lgc) to facilitate the Pearson correlation:

1284 **(a)** Alkenone-Sea Surface Temperatures (SST, ºC) of the core Gol-Ho1B_KSGC-31

1285 (Gulf of Lion: NW Mediterranean Sea (Sicre et al., 2016)), **(b)** Composite-plus-scaling

1286 (CPS) mean summer temperature anomaly reconstruction from tree rings records in

1287 Europe with respect to 1974-2003 CE (MSTA ºC) (Luterbacher et al., 2016), **(c)** LDI

1288 record along with reconstructed mean annual air temperatures (MAAT ºC) and mean

1289 annual air temperature anomalies with respect to 1979-2008 CE (MAATA ºC) for the last

1290 1500 years in LdRS, **(d)** Atlantic Multidecadal Oscillation (AMO) reconstruction (Mann

1291 et al., 2009), **(e)** Δ^{14}C in the atmosphere (reversed) (Reimer et al., 2013), **(f)** reconstruction

1292 of the difference of the total solar irradiance from the value of the PMOD composite

1293 series during the solar cycle minimum of the year 1986 CE (1365.57 W m^{-2}) (ΔTSI)

1294 (Steinhilber et al., 2009), **(g)** reconstructed concentration of atmospheric CH_4 (ppm)

1295 (Schmidt et al., 2011), and **(h)** reconstruction of the global volcanic aerosol forcing (W

1296 m^{-2}) (reversed) (Sigl et al., 2015). Acronyms: DA, Dark Ages; MCA, Medieval Climate

1297 Anomaly; LIA, Little Ice Age; MGW, Modern Global Warming. Blue bars show three

1298 low solar activity periods, the Spörer Minimum (SM), the Maunder Minimum (MM), and

1299 the Dalton Minimum (DM).

1300

1301
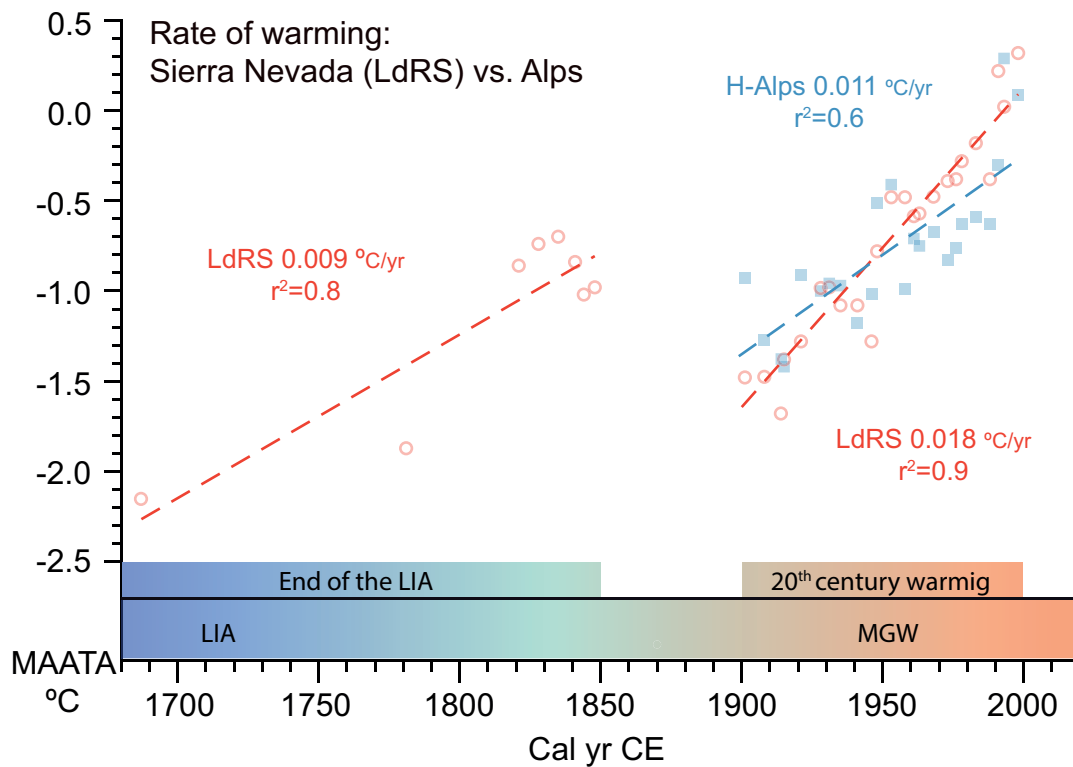
Figure 7. **Comparison between the average temperature warming rates from LdRS and the alpine areas of the Alps by means of ordinary least square regressions.** LDI-deduced MAATA (respect to the period 1979-2008 CE) from LdRS long and short cores for the last stage of the LIA and the 20th century (red open circles), and high-Alps historical (homogenised) temperature records from the Historical Instrumental Climatological Surface Time Series of the Greater Alpine Region (HISTALP) database (Auer et al., 2007; Böhm et al., 2010) at the same time averaging as LdRS shc-lgc to facilitate the comparison (blue closed squares).
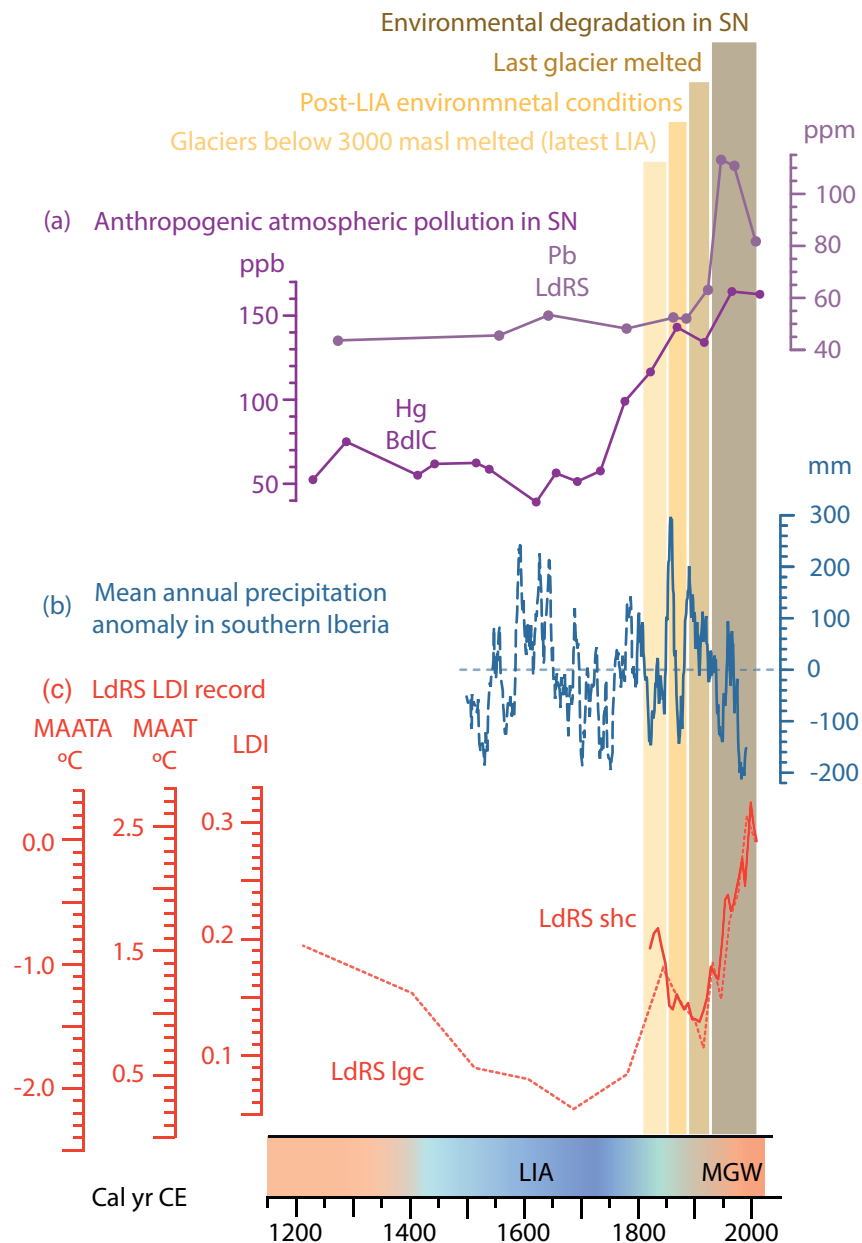
Figure 8. Comparison among different factors affecting the environmental evolution of alpine wetlands in the Sierra Nevada. (a) records of anthropogenic heavy metal atmospheric pollution (Pb and Hg) in two alpine sites of the Sierra Nevada: Laguna de Río Seco (LdRS) and Borreguil de la Caldera (BdlC) (Garcia-Alix et al., 2017; Garcia-Alix et al., 2013), **(b)** mean annual precipitation anomaly in southern Iberia from 1500 to 1990 CE with respect to the mean value of the instrumental period (1791-1990 CE): solid line- instrumental data from Gibraltar (southern Iberia); dashed line- anomaly precipitation reconstruction (Rodrigo et al., 1999), **(c)** LDI and reconstructed

1320   temperatures in LdRS. Colour bars indicate the four main environmental stages in the

1321   Sierra Nevada (SN) during the last 200 years. Acronyms: LIA, Little Ice Age; MGW,

1322   Modern Global Warming.